AGU PUBLICATIONS

Geochemistry, Geophysics, Geosystems

RESEARCH ARTICLE
10.1002/2014GC005540

Origin and evolution of the Kolbeinsey Ridge and Iceland Plateau, N-Atlantic

Bryndís Brandsdóttir[1], Emilie E. E. Hooft[2], Rolf Mjelde[3], and Yoshio Murai[4]

[1]Institute of Earth Sciences, Science Institute, University of Iceland, Reykjavík, Iceland, [2]Department of Geological Sciences, University of Oregon, Eugene, Oregon, USA, [3]Department of Earth Science, University of Bergen, Bergen, Norway, [4]Institute for Seismology and Volcanology, Hokkaido University, Sapporo, Japan

Key Points:
- The 700 km KRISE profile shows crustal structure between the KR and Aegir Ridges
- Extinct spreading centers coexisted with the extinct AEgir Ridge
- We constrain spreading history from the opening of the N-Atlantic to present

Correspondence to:
B. Brandsdóttir,
bryndis@hi.is

Citation:
Brandsdóttir, B., E. E. E. Hooft, R. Mjelde, and Y. Murai (2015), Origin and evolution of the Kolbeinsey Ridge and Iceland Plateau, N-Atlantic, *Geochem. Geophys. Geosyst.*, *16*, 612–634, doi:10.1002/2014GC005540.

Received 14 AUG 2014
Accepted 3 FEB 2015
Accepted article online 10 FEB 2015
Published online 4 MAR 2015

Abstract Variations in crustal structure along the 700 km long KRISE7 refraction/reflection and gravity profile, straddling 66.5°N across the Iceland Shelf, Iceland Plateau and western Norway Basin confirm that extinct spreading centers coexisted with the now extinct Ægir Ridge prior to the initiation of the Kolbeinsey Ridge at 26 Ma. The western 300 km of the profile, across the Iceland shelf, formed by rifting at the Kolbeinsey Ridge, whereas the eastern 400 km, across the Iceland Plateau and the western Norway Basin, formed by earlier rifting, possibly containing slivers of older oceanic or continental crust rifted off the central E-Greenland margin along with the Jan Mayen Ridge. Crustal thickness increases gradually across the Iceland shelf, from 12 to 13 km near the Kolbeinsey Ridge to 24–28 km near the eastern shelf edge, decreasing abruptly across the shelf edge, to 12–13 km. The Iceland Plateau has crustal thickness ranging from 12 to 15 km decreasing to 5–8 km across the western Norway Basin and 4–5 km at the Ægir Ridge. We suggest that high-velocity lower crustal domes and corresponding gravity highs across the Iceland plateau mark the location of extinct rift axes that coexisted with the Ægir Ridge. Similar lower crustal domes are associated with the currently active rift segments within Iceland and the Kolbeinsey Ridge.

1. Introduction

Tectonic evolution within the North Atlantic has been complex since the onset of spreading in late Paleocene-early Eocene [*Johnson and Heezen*, 1967; *Vogt and Avery*, 1974; *Talwani and Eldholm*, 1977; *Vogt et al*., 1980; *Srivastava and Tapscott*, 1986; *Larsen and Jakobsdóttir*, 1988; *Eldholm et al*., 1990; *Hopper et al*., 2003]. Whereas symmetric magnetic anomalies can be traced parallel to the Reykjanes Ridge and Mohns Ridge back to Chrons C24 and C22, respectively, anomalies within the Iceland Plateau (IP) and Ægir Ridge in the Norway Basin, as well as along the Greenland-Iceland-Faeroe Ridge, are irregular, reflecting rift jumps and multiple-branched crustal accretion zones, details of which still remain unresolved (Figure 1). Data from early bathymetric, magnetic, gravimetric, and seismic surveys [*Johnson and Heezen*, 1967; *Vogt et al*., 1970; *Bott*, 1971; *Johnson and Tanner*, 1972; *Meyer et al*., 1972; *Pitman and Talwani*, 1972; *Eldholm and Windisch*, 1974; *Vogt and Avery*, 1974; *Kodaira et al*., 1998a] and DSDP leg 38 [*Talwani and Udintsev*, 1976; *Kharin et al*., 1976; *Talwani and Eldholm*, 1977; *Grønlie et al*., 1979; *Weigel et al*., 1995] constrained matching structural and stratigraphic features along the continental margins of Norway and Greenland and identified the Jan Mayen Ridge (JMR) as being a sliver of continental crust, conjugate to the Møre Margin, Norway, formed as a result of a westward rift jump that activated the Kolbeinsey Ridge at about 26 Ma (Chron C7), late Oligocene time [*Gradstein et al*., 2012]. Whether the initiation of the Kolbeinsey Ridge took place in a single event or multiple phases has been debated in the literature [*Johnson and Heezen*, 1967; *Johnson and Tanner*, 1972; *Talwani and Eldholm*, 1977; *Vogt et al*., 1980; *Nunns*, 1982; *Bott*, 1985; *Srivastava and Tapscott*, 1986; *Eldholm et al*., 1990; *Kodaira et al*., 1998a, 1998b; *Jung and Vogt*, 1997; *Müller et al*., 2001; *Mjelde et al*., 2002] and plate boundary complications associated with rifting at the Ægir Ridge have not been studied in any detail.

Geomagnetic data collected in the 1970s revealed irregularities in spreading rates and rift dislocations within the Norway Basin where the apparent fan-shaped magnetic anomaly pattern along the extinct Ægir Ridge is considered to reflect a gradual decrease in the rate of spreading southward, between Chrons C23 and C7 [*Talwani and Eldholm*, 1977; *Grønlie et al*., 1979], i.e., ~53–25 Ma [*Gradstein et al*., 2012; *Ogg*, 2012] or between Chrons C21n and C13n [*Jung and Vogt*, 1997], 47.35–33.7 Ma [*Ogg*, 2012], prior to the initiation of the Kolbeinsey Ridge. Although poorly constrained by the magnetic data (Figure 1b), a southward decrease

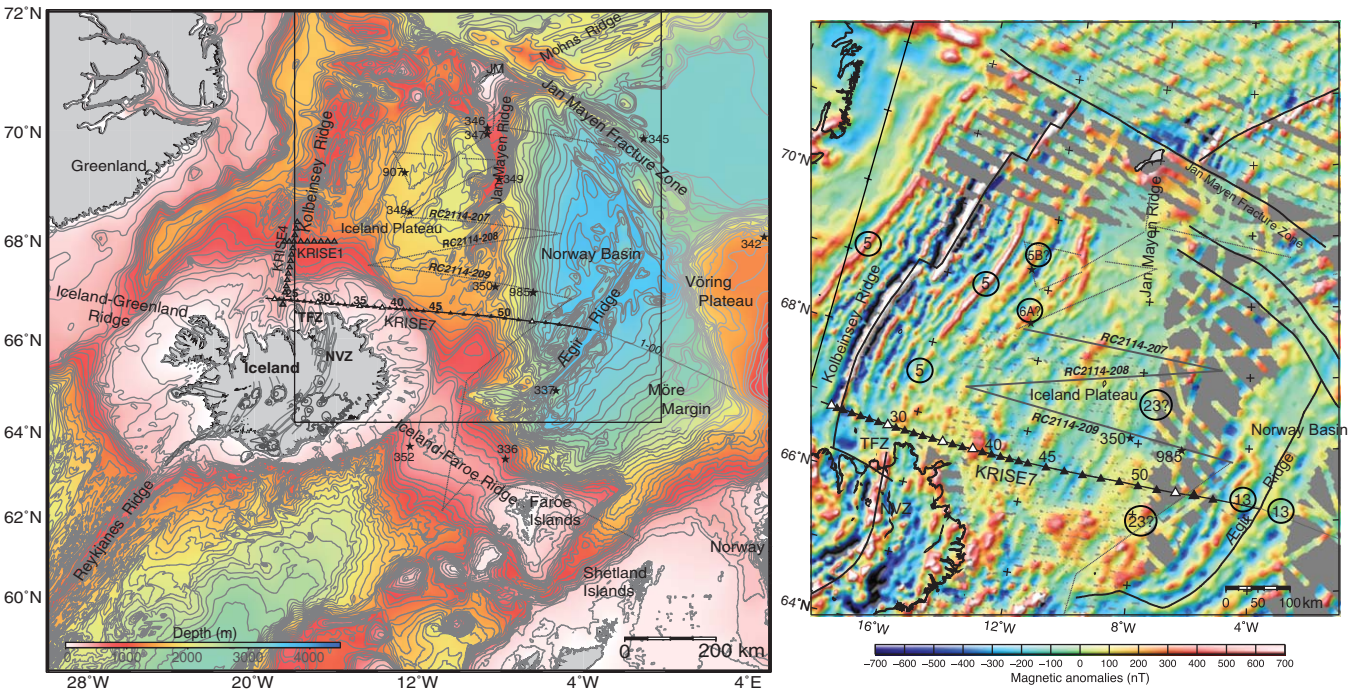

Figure 1. Location of the KRISE seismic reflection/refraction experiment, offshore N-Iceland. (a) GEBCO-bathymetry at 200 m contour interval. The 700 km long EW profile (KRISE7), straddles 66.5°N across the Iceland Shelf, Iceland Plateau and western Norway Basin. Older reflection profiles (gray lines) across the eastern Iceland Plateau were surveyed by R/V Conrad cruise RC2114-1978. The KRISE7 profile joins up with a conjugate reflection-refraction profile (1-00) east of the Ægir Ridge [*Breivik et al*., 2006]. Black triangles show OBS locations (white for no data) and gray triangles stations along the KRISE1 and KRISE4 profiles. Airgun shots were fired along the black line. DSDP and IODP core sites, black stars. Tjörnes Fracture Zone (TFZ) and Northern Volcanic Zone (NVZ). The tectonic map of Iceland is based on *Einarsson and Saemundsson* [1987]. Black box outlines magnetic anomaly map, shown in (b). Black lines indicate rift axis and major transform zones. Circled numbers refer to magnetic anomalies. Areas devoid of data are gray.

in spreading rate along the Ægir Ridge must have been compensated by another rift axis further west, along the eastern margin of the IP, as initially suggested by *Talwani and Udintsev* [1976], thus forming a parallel spreading center with the Ægir Ridge. Despite its vital role in the plate tectonic evolution of the N-Atlantic region, the second arm of the Ægir Ridge has been largely ignored in more recent tectonic compilations. Tectonic models assume rifting west of the Jan Mayen Ridge to have commenced as early as Chron C20 [*Bott*, 1985], (45.7 Ma, [*Ogg*, 2012]) or between Chrons C18 and C13 (∼41–33 Ma, [*Ogg*, 2012]), triggered by the Iceland plume [*Müller et al*., 2001]. However, magnetic anomalies older than Chron C6 (∼19–24 Ma, [*Ogg*, 2012]) have not been identified west of the Kolbeinsey Ridge [*Vogt et al*., 1980; *Weigel et al*., 1995]. Although complicated rifting within the eastern IP has obscured the magnetic lineation pattern, Chrons C18–C20 (∼41–45.7 Ma, [*Ogg*, 2012]), formed at the RR are now located southeast of Iceland, suggesting a middle Eocene age for some of the eastern margin of the IP.

While it has been proposed that the Jan Mayen microcontinent may extend into eastern Iceland [*Fedorova et al*., 2005; *Leftwich et al*., 2005; *Foulger*, 2006], the southern Jan Mayen Ridges, within the Iceland Plateau all appear oceanic in origin. Data from early seismic reflection surveys south of the JMR revealed basement ridges inferred to be of continental origin to the north and oceanic origin to the south [*Talwani and Udintsev*, 1976; *Gairaud et al*., 1978; *Grønlie et al*., 1979]. The oceanic origin of the easternmost basement ridge, south of the JMR, was confirmed by the recovery of basalts from DSDP hole 350, 200 km west of the Ægir Ridge axis. These basalts have light REE patterns similar to the Vøring Plateau basalts (DSDP hole 342) and the lower and middle Faeroe basalt series [*Schilling*, 1976]. K-Ar dates of 40–44 Ma [*Kharin et al*., 1976] support simultaneous middle Eocene formation of these basalts. Although there is consensus regarding the formation of the JMR, its volume and southern extent into the Iceland Plateau has remained unresolved [*Gaina et al*., 2009; *Breivik et al*., 2012]. The origin of the Iceland Plateau and the location of any western rift axes suggested to have coexisted with the Ægir Ridge have been poorly resolved as limited data exists within this region.

We present refraction and reflection data along a profile straddling 66.5°N across the northern Iceland Shelf and southeastern Iceland Plateau. The 700 km long profile, along the KR spreading direction (105°, [*DeMets*

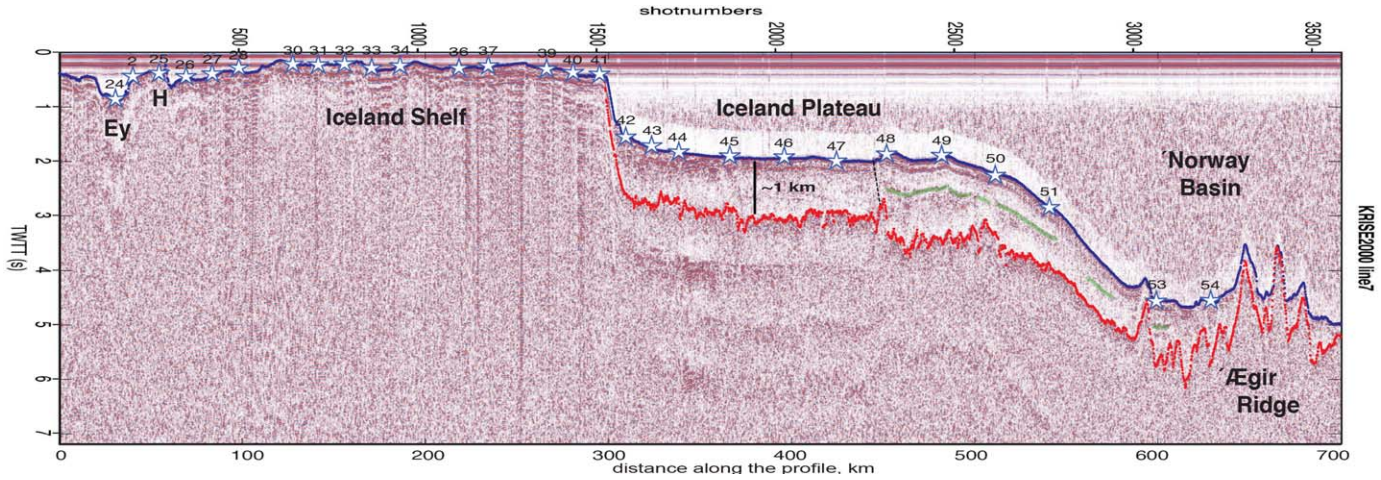

Figure 2. KRISE7 reflection section, bandpass filtered 20–40 Hz with a 48 dB/oct drop-off and plotted with an AGC window of 1 s. Seafloor picks are blue and basement picks red. OBS stations with data, white stars. Green picks mark reflector R2, dashed line is an unconformity. Within the TFZ, the Eyjafjardarálll basin (Ey) marks the southern continuation of the Kolbeinsey Ridge, and the Hllinn (H) volcanic system the northward continuation of the NVZ. The Iceland Shelf has thin sediment cover whereas sediment thickness of 1–1.5 km (1–1.5 s) characterizes the Iceland Plateau.

et al., 1994]), measured variations in crustal structure and thickness, as an indication of melt flux from the initial opening of the N-Atlantic, at the now extinct Ægir Ridge, to the current plate boundary. The western 300 km of the profile lies across the Iceland Shelf and is considered to have formed by rifting at the Kolbeinsey Ridge. The eastern 400 km cross the Iceland Plateau and Norway Basin, a region formed by rifting at the Ægir Ridge and at the IP rift axis along the former central E-Greenland margin. With combined modeling of seismic and gravity data, we constrain crustal formation and the spreading history from the opening of the N-Atlantic in the early Eocene to present. Complicated extensional tectonics at the eastern margin of the Iceland Plateau seem to be accommodated by smaller rifts and extensional basins with parallel spreading centers; a geometry similar to the present tectonic configuration of the Iceland rift zones.

2. The KRISE Data Acquisition: The Experiment

Three seismic/magnetic/gravity profiles were surveyed in June 2000, a 230 km line just east of the Kolbeinsey Ridge [*Hooft et al*., 2006], and 138 and 700 km cross-axis lines located 180 km [*Furmall*, 2010] and 70 km north of the Icelandic coast, respectively (Figure 1). The data were acquired using 33 Japanese Ocean bottom seismometers (OBSs) owned by Hokkaido University using the University of Bergen research vessel Håkon Mosby and the Icelandic Coast Guard Cutter Ægir. The OBSs along the 700 km KRISE7 profile were placed at 10 km intervals across the ridge axis, 15 km intervals along the Iceland Shelf, and 30 km intervals across the Iceland Plateau and Norway Basin. The KRISE7 profile joins up with a conjugate reflection-refraction profile east of the Ægir Ridge [*Breivik et al*., 2006].

Each OBS was equipped with a three-component gimbal-mounted geophone (one vertical and two horizontal) with 4.5 Hz resonance frequency [*Kanazawa and Shiobara*, 1994]. A four-element airgun array with a total volume of nearly 79 L (4800 cubic inch) towed at 8 m depth constituted the seismic source. Shots were spaced at 180 m intervals, corresponding to a shot rate of approximately 70 s, in order to minimize water-column reverberations. Shot positions were obtained using the shipboard Global Positioning System.

Single-channel streamer data were acquired along all profiles in order to determine the seafloor and basement depths (Figure 2). After bandpass filtering, the data between 20 and 40 Hz with a 48 dB/oct dropoff, we selected an AGC window of one second in order to bring out the strong basement reflection we observe east of the Iceland Shelf. On the shallow Iceland shelf, this reflection is obscured by several strong water-column multiples.

The OBS depths along the KRISE7 profile range from 138 to 632 m across the Iceland shelf, 1172 to 1454 m across the Iceland Plateau, and deepen to 3354 m at the Ægir Ridge Axis. The largest sources of uncertainty are OBS position, identification of arrival time, and timing error. Given the shallow water depths at the

Iceland Shelf, other than ranging each station several times, no comprehensive attempt was made to relocate these OBSs before recovery. OBSs in the Norwegian Sea were triangulated before release. In addition, a grid search method [*Hooft et al*., 2006] was used to relocate the OBSs, and simultaneously solve for the water velocity and timing shifts. The water velocity was relatively low (1450–1460 m/s) across both the Iceland shelf and Iceland Plateau but higher (1460–1480 m/s) in the deeper water of the Norwegian Basin and at the Ægir Ridge. The location accuracy is close to 50 m along the profile, the stations were shifted 58 m on average, with a range from 79 m to the west to 218 m to the east. The average time shift was about 35 ms, excluding OBS 27, OBS 43, and OBS 46 where the time shifts were 100, 338, and 661 ms, respectively. Inaccurate clock calibration caused a large time shift for OBS 43 as the instrument did not surface when released but was retrieved 5 days later. The clock calibration or initial recording of OBSs 27 and 46 seems to have been flawed.

3. Seismic and Gravity Data Modeling

Very favorable weather conditions during the survey provided optimum signal-to-noise ratios for both reflection and refraction data. Of the 33 instruments deployed, the westernmost OBS (23) did not surface and usable data could not be retrieved from four other instruments. Selected record sections from the 28 OBSs used to invert for crustal structure and thickness are shown in Figure 3. We recorded high-quality refraction data out to a range of up to 150 km. Clear crustal refraction phases were observed on all the instruments and Moho reflections were observed on most stations. Mantle-refracted phases (Pn) were observed on stations west of the Ægir Ridge. To pick travel times of crustal and upper mantle refraction phases (P and Pn) and Moho reflection (PmP) arrivals, the OBS data was bandpass filtered from 3 to 20 Hz, and 3 to 8 Hz, respectively. A total of 20,367 refractions and 1851 reflections were picked manually and assigned a picking error of 25 ms and 50 ms.

The travel time data were inverted to construct a two-dimensional crustal velocity model and depth to Moho using the method of *Korenaga et al*. [2000]. This method performs a joint refraction and reflection travel time tomography inversion to simultaneously invert for the seismic velocity field and depth of a single reflecting interface. The forward problem is solved by a hybrid method using the shortest path [*Moser*, 1991] and the ray-bending method [*Moser et al*., 1992]. The inverse problem uses a sparse least squares method [*Paige and Saunders*, 1982] to solve a regularized linear system.

Crustal-refracted P phases were initially inverted using a velocity-depth model based on the previously analyzed KRISE4 line parallel to the Kolbeinsey Ridge, the FIRE line across NE-Iceland [*Hooft et al*., 2006; *Staples et al*., 1997], and measured compressional velocities of 1.7–2.3 km/s in DSDP cored sediments within the N-Atlantic region [*Gairaud et al*., 1978]. Subsequently, a two-dimensional inversion of crustal structure was performed using the best-fit velocity-depth profile as a starting model. The velocity model was parameterized as a sheared mesh hanging from the seafloor topography with a 1 km horizontal node spacing and depth nodes spaced incrementally from 50 m near the seafloor to 1 km at 30 km depth. The Moho was parameterized as a floating reflector with nodes every 2 km with one degree of freedom in the vertical direction. The inversion was regularized with smoothing constraints that are imposed using weighted correlation lengths. For the velocity model, we used a depth-dependent horizontal correlation length that increased linearly from 1 km at the seafloor to 10 km at the bottom of the model ($\sim$28 km below the seafloor), and a vertical correlation length that also increased linearly from 0.1 km at the seafloor to 2 km at the bottom of the model, both weighted by different factors ranging between 1100 and 1700. The correlation length for the depth nodes of the reflector was 9 km, weighted by a factor of 10. The depth sensitivity was also weighted by a depth kernel weighting parameter (w), which was typically set to 1 to weight PmP and Pg arrivals equally. As a test of the trade-off between lower crustal velocity structure and Moho topography, we explored the effect of $w = 10$ and 100 and found that the inversion results were not sensitive to the value of the depth kernel weighting parameter. Ten iterations were performed for each starting model.

Damping was used to diminish velocity perturbation artifacts in the model. As most rays turn within the uppermost 10 km, we applied higher levels of damping below that depth, resulting in a smoother model with depth. We tested inversion damping parameters, rejecting more complex velocity models, which did not appear to be geologically reasonable. To explore the model space, we have run several tens of inversions for a range of inversion parameters and travel time files. Our best fitting models (Figure 4a) have an

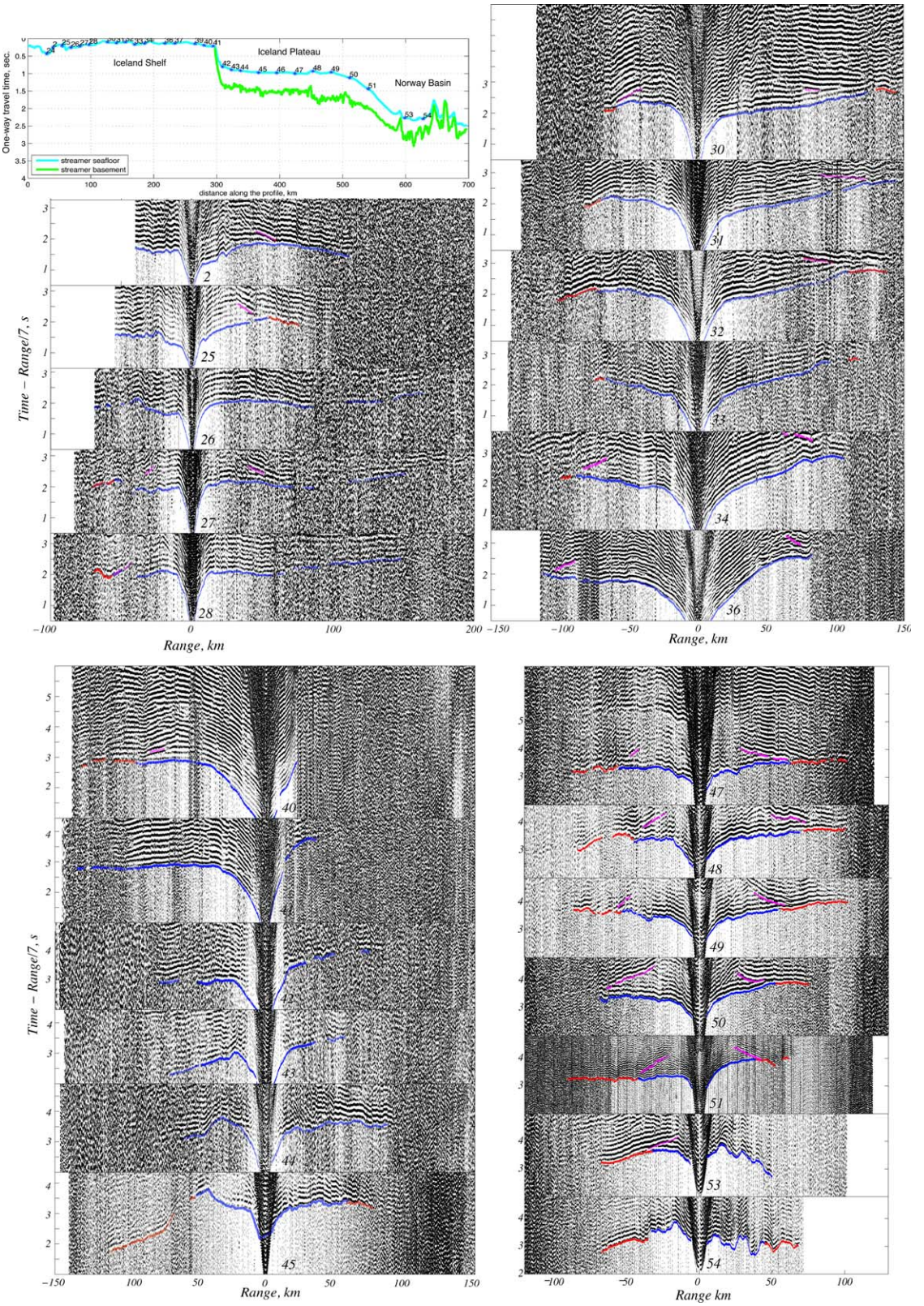

Figure 3. KRISE7 bathymetry profile and record sections from OBSs on the Iceland Shelf (OBSs 24–41), Iceland Plateau (OBSs 42–51), and Norway Basin (OBSs 51–54), plotted with a reduction velocity of 7.0 km/s versus range. Data are band-pass filtered from 3 to 20 Hz and amplified as a function of range. Arrivals are observed out to over 100 km. Semitransparent markings denote the picked travel times of Pg (blue), PmP (purple), and Pn (red). Note clear PmP arrivals on the eastern IP margin (stations 47–51).

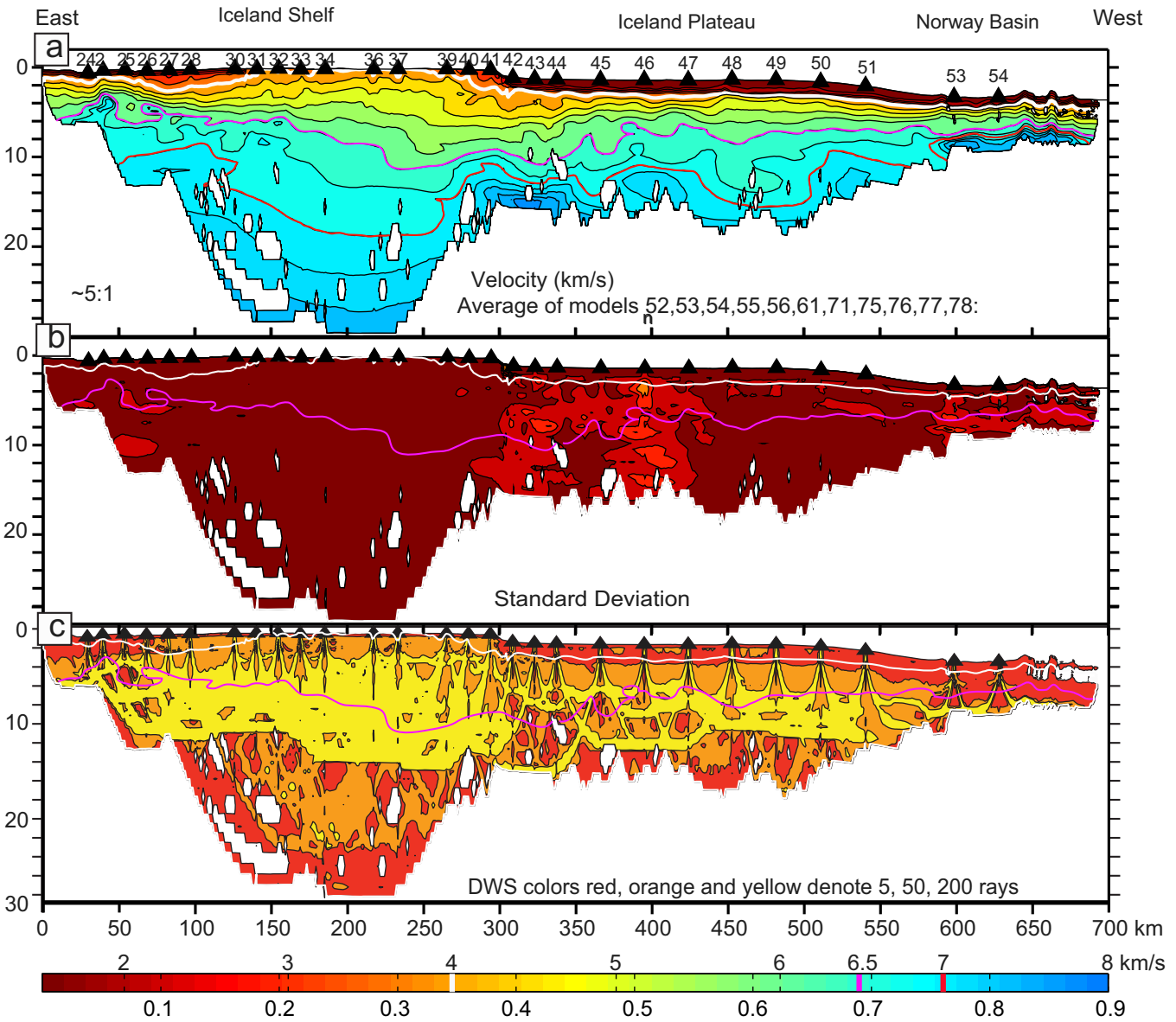

Figure 4. (a) Average of 11 best fitting crustal models. Sediment-basement boundary (isovelocity contour 4 km/s), upper lower crustal boundary (isovelocity contour 6.5 km/s), and isovelocity contour 7 km/s are indicated with white, purple, and red lines, respectively. (b) Velocity anomalies relative to the mean velocity-depth model. Black line represents modeled Moho topography with standard deviation (dashed lines). (c) Mean derivative weight sum (DWS, a proxy for ray density), for the velocity model showing dense P and PmP ray coverage (≥200, yellow and ≥50 orange) along the profile.

average root mean square (RMS) travel time residual of 34 ms for P and 48 ms for PmP and chi-squared average of (χ^2) of 1.12 for P and 1.0 for PmP, where

$$\chi^2 = \frac{1}{(N-1)} \sum_{i=1}^{N} \left(\frac{t_{i,obs} - t_{i,calc}}{\sigma_i} \right)^2$$

and $t_{i,obs}$, $t_{i,calc}$, and σ_i are the observed and calculated travel time and standard deviation for the ith of a total of N observations.

The average and standard deviation of 11 inversions provides an idea of where model recovery is stable versus where the model is less well constrained (Figure 4b). The crustal velocities are consistently recovered except beneath the westernmost Iceland Plateau near the edge of the Iceland Shelf (275–425 km along the profile). The model resolution at any point is a function of the number of crossing rays as well as relative

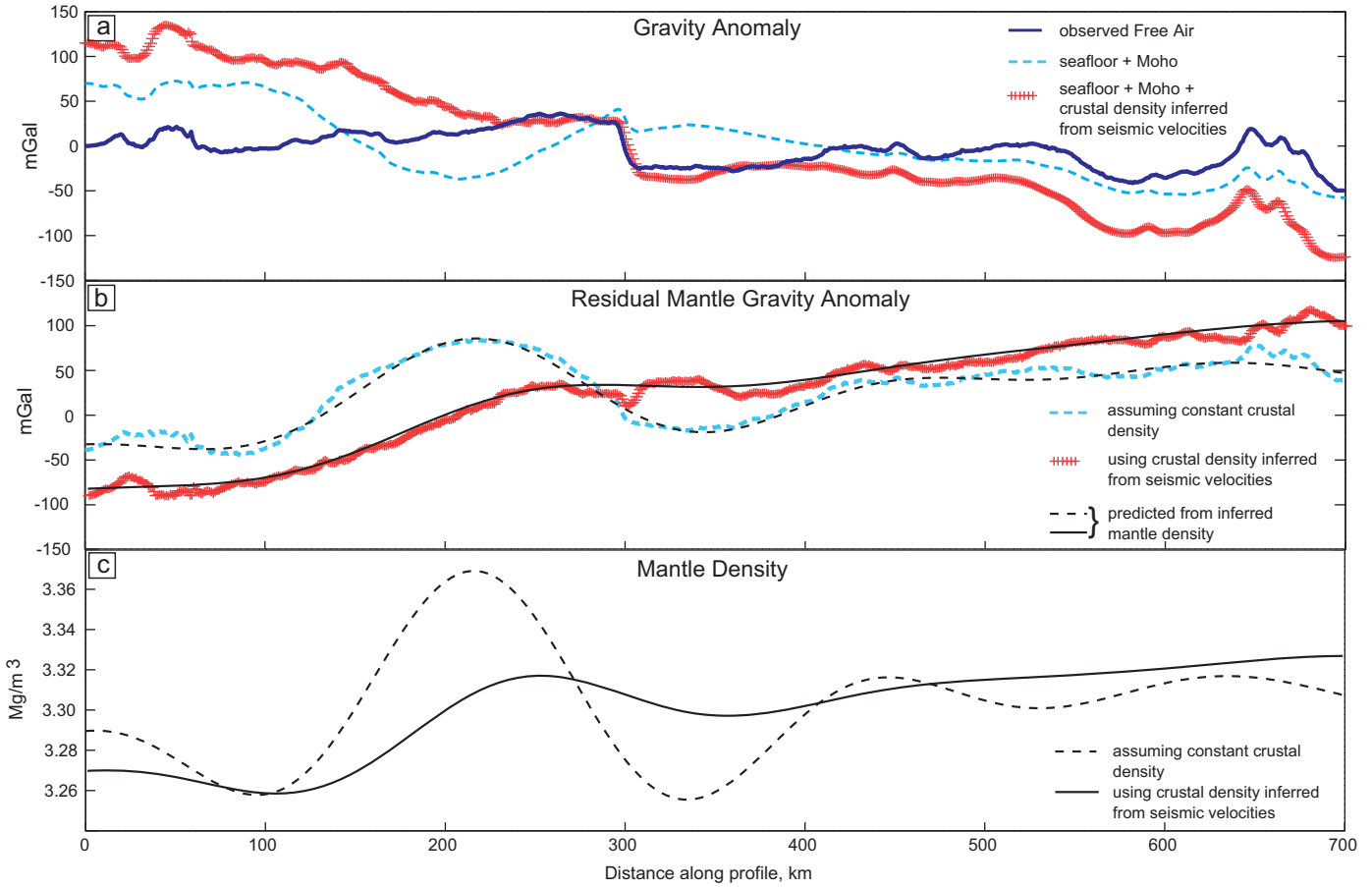

Figure 5. (a) Free air gravity anomaly and predicted gravity anomalies, (b) residual mantle gravity anomaly, and (c) mantle density plotted as a function of distance along the profile. (a) The observed Free Air Gravity anomaly (blue solid line) is compared to the predicted gravity anomaly for the seafloor and Moho topography using constant crustal density (dashed light blue line) and variations in crustal density inferred from seismic velocity variations (red crosses); see text for discussion. (b) The residual mantle gravity anomaly is calculated by subtracting the predicted gravity anomaly due to the crustal structure shown in Figure 5a from the observed Free Air anomaly both for constant and varying crustal density; same line styles as in Figure 5a. Figure 5c Mantle density anomalies are calculated by downward continuation of the residual mantle gravity anomaly using a compensation depth of 100 km and a band-pass filter from 150 to 1000 km for both constant crustal density (dashed line) and varying crustal density (solid line). The component of the residual mantle gravity anomaly that is accounted for by the mantle densities variations inferred in Figure 5c is also shown in Figure 5b (solid and dashed black lines). Note the gradual decrease in mantle density toward Iceland in the west.

raypath orientations, approximated by the derivative weight sum (DWS), which is a weighted sum of the length of ray paths that influence each model parameter [*Toomey et al*., 1990]. The greater variability in recovered velocity off the Iceland Shelf reflects uncertainty of the smaller wavelength features of the model due to smaller ray coverage on stations near the Shelf edge (Figure 4b). Remaining portions of the model are recovered with remarkable consistency with velocities that typically vary less than 0.1 km/s. For this suite of models, Moho recovery is also very consistent except the western 100 km of the Iceland plateau that is closest to the Iceland shelf, between 300 and 400 km along the profile, where there is greater variability in recovered Moho depth (standard deviation of $\pm$1.2 km versus a typical value of $\pm$400 m elsewhere along the profile).

In Appendix A, we investigate the resolution of our model by testing the resolution of specific observed structures, and by using checkerboard tests. These tests are consistent in showing that the resolution of the crustal model depends primarily on the instrument spacing, the ray coverage, and the velocity gradients. We conclude that the uppermost 12–20 km of the crust are best resolved based on maximum depth propagation of compressional waves to 18–20 km beneath the Iceland shelf and to 12 km on the Iceland Plateau and that major crustal velocity perturbations are well resolved.

We calculate the contribution of the crustal structure to the observed free air gravity anomaly (Figure 5a) to infer density variations in the mantle. We first remove the effect of the seafloor topography, the crustal

density structure, and the Moho topography from the free air gravity data to obtain the residual mantle gravity anomaly (Figure 5b). We convert crustal seismic structure to density in two ways. First, we assume that the crust has a uniform density of 2850 Mg/m^3. Second, we calculate crustal density from seismic velocity using the relationship of *Carlson and Raskin* [1984] for diabase and gabbros. The baseline mantle density is 3240 Mg/m^3 similar to that determined beneath the Reykjanes Ridge [*Weir et al*., 2001]. A smoother residual mantle gravity anomaly is obtained when crustal density is inferred from seismic velocity than when constant crustal density is assumed; this is not surprising given the relatively large lateral variations in thickness of the different crustal seismic layers. We find that the calculated residual mantle gravity anomaly decreases by about 150–200 mGal from the ÆR toward the KR (Figure 5b).

Variations in the residual mantle gravity anomaly may be attributed to density variations in the mantle. To infer mantle density variations, we downward continue the residual mantle gravity anomalies using the method of *Parker and Huestis* [1974] (as coded by [*Korenaga et al*., 2001]). The compensation depth is taken to be 100 km. To stabilize the downward continuation, the smallest wavelength residual mantle gravity anomaly used is 150 km. We infer that mantle densities decrease by about 60–70 kg/m^3 (0.06–0.07 Mg/m^3) toward Iceland (Figure 5c). The predicted mantle density variation accounts for the long-wavelength component of the residual mantle gravity anomalies (Figure 5b). A baseline mantle density of 3.27 Mg/m^3 is 0.03 Mg/m^3 higher than along the Reykjanes and Kolbeinsey Ridges, where a decrease in mantle density toward Iceland is also observed [*Weir et al*., 2001; *Hooft et al*., 2006]. The decrease in mantle densities beneath the Iceland shelf is consistent with an increase in mantle temperatures by about 200°C, in line with *Shorttle et al*. [2014] who found that an excess mantle potential temperature of $\geq$130°C is required in order to generate the 20 km thick Icelandic crust. An upper mantle density of 3.27 Mg/m^3 may represent lower density harzburgite and lherzolite rather than higher density pyroxenite or eclogite.

Using the approach of [*Korenaga et al*., 2002; *Korenaga and Sager*, 2012], we calculated average lower crustal seismic velocity to assess possible variations in mantle dynamics, from the initiation of spreading within the N-Atlantic to present day rifting, north of Iceland. We applied a pressure correction of 0.22×10^{-3} km/s/MPa and temperature correction of -0.5×10^{-3} km/s/°C prior to calculating average lower crustal velocity (LCV) below an isovelocity of 6.7 km/s at a spacing of one km. For the geotherm, we assumed 10°C at the seafloor and 800°C at the Moho. Decreasing the Moho temperature from 800 to 500°C lowers the average LCV by about 0.1 km/s. However, as fluid dynamical and geochemical models of mantle upwelling and evolution at volcanic margins during continental breakup are presently not compatible [*Nielsen and Hopper*, 2004; *Sleep*, 2007; *Korenaga*, 2004], variations in lower crustal velocities versus total crustal thickness should be taken as indicators of the relative magnitude of active versus passive mantle upwelling processes, see discussion below.

4. Results

We separate our model description into the three physiographic provinces that characterize the region north and northeast of Iceland (Figures 1 and 2). The first region, the youngest portion of the KRISE7 profile (from 0 to 300 km) is the shallow Iceland Shelf, formed at the KR since about 26 Ma, becoming older eastward. The western end of the profile lies across the Eyjafjardaráll basin, the magma-starved southern extension of the KR. The second region, between 300 and 500 km, crosses the Iceland Plateau (IP), which lies north of the Iceland Shelf and the Iceland-Faeroe Ridge and is bounded by the KR to the west, the Jan Mayen Fracture Zone to the North, and the Norway Basin to the east (Figure 1). The third region, between 500 and 700 km along the KRISE7 profile, covers the IP slope into the deep western Norway basin where the crust becomes younger and deeper eastwards, toward the abandoned ÆR.

4.1. Crust Generated at the KR, 0–300 km, Comparison With Iceland

Crustal formation at the KR from its initiation to the present records significant lateral variations in compressional velocity (Figures 4 and 6), especially along the westernmost 150 km, i.e., across crust formed by spreading at the KR during the last ~15 Ma, based on NUVEL-1a half-spreading rates [*DeMets et al*., 1994]. This is partly because the westernmost 100 km cross parallel spreading structures within the complex Tjörnes Fracture Zone, the magma-starved Eyjafjardaráll (Ey) extensional basin (650 m depth), and volcanic systems further east that form the offshore continuation of the Northern Volcanic Zone in Iceland.

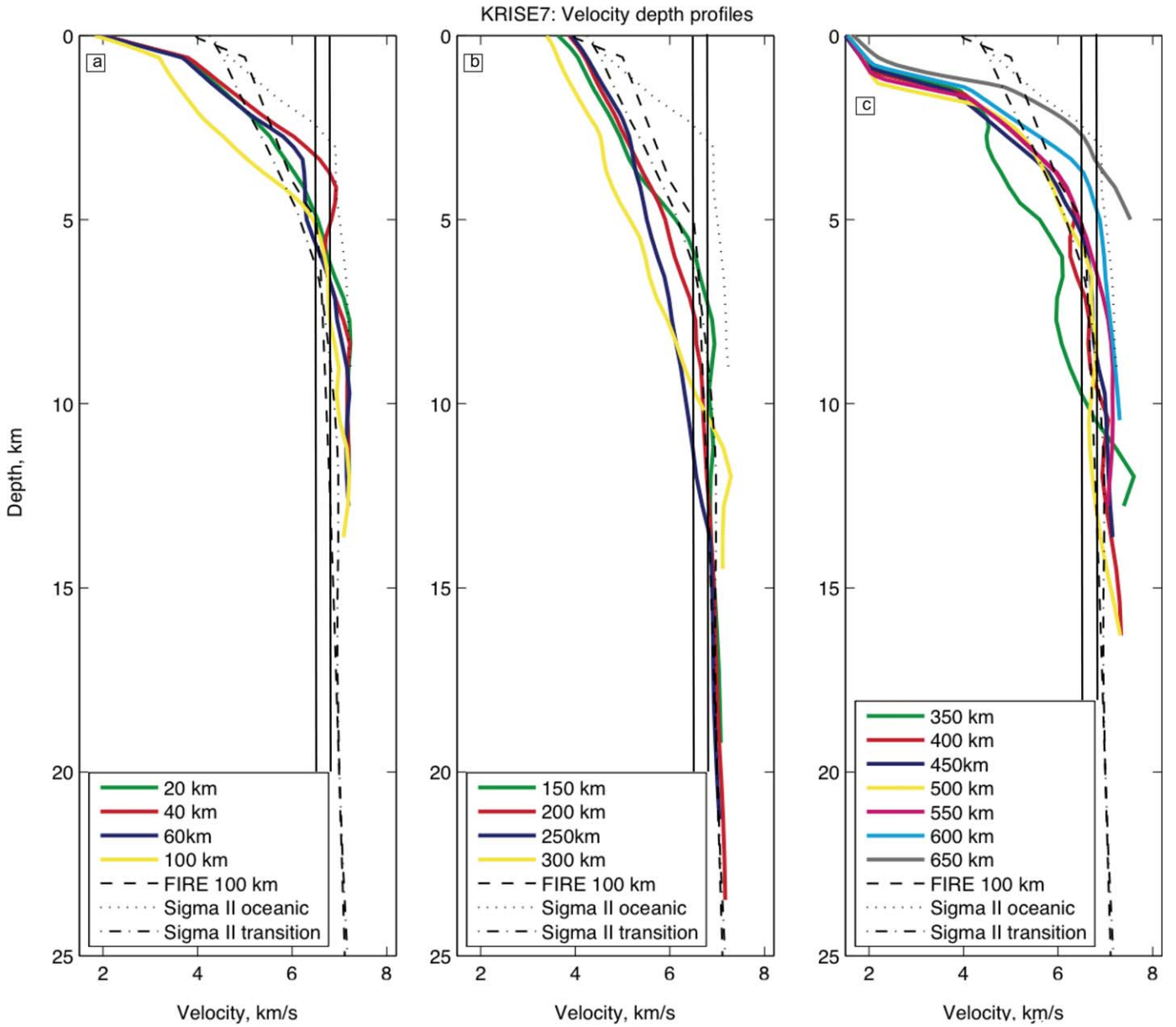

Figure 6. Plots of 1-D velocity-depth profiles averaged over 20–50 km sections of the KRISE7 transect (Figure 4), color coded by distance. Average 1-D velocity structure of the FIRE profile in E-Iceland [*Staples et al.*, 1997] and Sigma II profile along the SE-Greenland margin [*Korenaga et al.*, 2000, 2001] are shown for comparison. Vertical lines are at 6.5 and 6.8km/s. Note similarities in crustal velocities below 10 km depth.

On the Iceland shelf, surface velocities range from 2.7 to 4.5 km/s, indicative of both glacial deposition and basal erosion. Surface compressional velocities of 2.7–4.5 km/s observed on Iceland [*Pálmason*, 1971; *Brandsdóttir and Menke*, 2008] correlate with geological formations ranging from glacially derived material and recent volcanic extrusives, basalts, and hyaloclastites to compacted basalts of eroded Tertiary regions. The 1–2 km thick layer with compressional velocities of 2.5–4.0 km/s within an ~80 km wide basin along the westernmost part of the profile (between OBS stations 25 and 30), most likely represents glacial sediments deposited during the Last Glacial Maximum when ice-streams from the Iceland ice cap extended out to the shelf edge [*Norddahl et al.*, 2008]. Furthermore, the fan-shaped formation at the steep shelf edge (beneath OBS stations 41 and 42) is similar to the progressive glaciomarine fan at the SE-Greenland margin [*Korenaga et al.*, 2000; *Hopper et al.*, 2003]. In contrast, the depth to isovelocity contour 4 km/s varies between 1 and 2.5 km depth across the westernmost 125 km of the KRISE7 line, and breaches the surface on the eastern Iceland Shelf (Figures 6a and 6b). Surface velocities of 4–4.5 km/s characterize the eroded

Tertiary basement of Iceland and the Iceland-Faeroe Ridge [*Pálmason*, 1971; *Flóvenz and Gunnarsson*, 1991; *Staples et al*., 1997; *Menke et al*., 1996; *Darbyshire et al*., 1998; *Smallwood et al*., 1999].

Assuming a fairly uniform production of extrusives with time, a 1.5 km range in depth of isovelocity contour 4 km/s is in agreement with estimates of basement erosion of at least 1.5 km inferred from zeolite zonations in E-Iceland [*Saemundsson*, 1986]. Although devoid of sediments, the outer shelf (east of anomaly 5, ~10 Ma) has a weak magnetic field (Figure 1), [*Vogt et al*., 1980] in contrast to Eastern Iceland where magnetic anomalies are quite pronounced. The weaker magnetic field on the outer shelf might be related to a sheeted dike complex (layer 2B) which has significantly lower magnetization than the extrusive and shallow intrusive layer 2A [*Lowrie*, 1979]. We infer that on the eastern Iceland Shelf significant glacial erosion (1.5–2.5 km) has removed the uppermost crust, exposing the sheeted dikes complex.

The upper/lower crustal interface beneath Iceland has been defined by an abrupt change in velocity gradients ranging from 6.5 to 6.8 km/s [*Flóvenz and Gunnarsson*, 1991; *Staples et al*., 1997; *Weir et al*., 2001]. A similar range is observed along the KRISE profile, where an abrupt change in velocity gradients at 6.8 km/s and is observed near the present plate boundary (Kolbeinsey Ridge) decreasing to 6.5 km/s 100 km further east along the profile (Figures 6a and 6b). Discussion of upper crustal thickness, below is based on the classical definition of layer 2/3 boundary, at 6.5 km/s although we also explore higher velocities in association with modeling of mean velocities within the lower crust.

The upper crust (layers 1 and 2, depth to isovelocity contour 6.5 km/s) is thinnest across the divergent plate boundary, south of the KR, and across the volcanic systems within the TFZ (Figure 1), and thickens with age, off-axis. This pattern is similar to that in Iceland. The upper crust has been generated by submarine extrusions and possibly subaerial volcanism during the initiation of the KR. Shallow seafloor multiples, however, prevent identification of seaward dipping reflectors within the KRISE7 reflection data. Upper crustal thickness has an average range of 4–6 km along the westernmost 150 km of the profile, increasing gradually to nearly 12 km beneath the NE Iceland Shelf. Within Iceland, an upper crustal thickness in excess of 10 km has only been observed at the southern propagating tip of the Eastern Volcanic Zone [*Flóvenz and Gunnarsson*, 1991]. Receiver functions infer a 5.5–6.5 km thick upper crust and 25–30 km total crustal thickness beneath the southeastern coast of Iceland [*Du and Foulger*, 2001]. This region is also adjacent the edge of the Iceland Shelf, and thickened upper crust may be a characteristic feature of the outer Iceland Shelf.

Based on wide-angle reflections (PmP), the crustal thickness decreases from 25–30 km at the NE Iceland Shelf (150–250 km), to 12–14 km offshore N-Iceland (60–110 km). Our modeled crustal thickness is a minimum thickness since the broad high-velocity anomalies (7.4–8.2 km/s) at the base of the crust near the shelf edge are not thoroughly resolved by our data and may represent a complex crust-mantle transition zone. The depth to isovelocity contour 7 km/s ranges from 8–9 km at the western end of the line (40–130 km) to ~19 km beneath the central Iceland Shelf (130–260 km). The lower crustal structure and crustal thickness of the Iceland Shelf is similar to what has been observed along the Iceland-Greenland and Iceland-Faroe Ridges [*Smallwood et al*., 1999; *Holbrook et al*., 2001] and in the Tertiary regions of Iceland [*Staples et al*., 1997; *Darbyshire et al*., 1998; *Allen et al*., 2002; *Du et al*., 2002] (Figure 6).

The upper/lower crustal thickness ratio (between isovelocity contour 4 km/s, 6.5 km/s and Moho, white, purple, and black lines on Figure 4) varies from 1:1 to >1:4 across the Iceland Shelf reflecting considerable variations in extrusion versus intrusion rates throughout the last 25 Ma (Figures 6a and 6b). Assuming symmetric spreading at present KR rates (1.8 km/Ma), the thicker crust beneath the NE Iceland Shelf (100–275 km along the profile) was generated between 9–10 and ~25 Ma. During this period, a 8–14 km thick lower crust of velocities 7–7.6 km/s was created under the influence of increased melt flux, discussed below. The decrease in Layer 2 thickness (isovelocity contours 4–6.5 km/s) and crustal thickness towards the current plate boundary may reflect a gradual decrease in melt production since the initiation of the KR. Variations in intrusion/extrusion rates and plate boundary complications (repeated rift jumps) need also be considered.

Increased mantle decompression and increased melt flux are related processes that both enhance melt production. An increase in mantle potential temperature will raise average crustal velocities through increased magnesium and decreased silica content, whereas igneous crust generated by increased melt flux (active, plume driven upwelling) has a fairly constant chemical composition/seismic velocity, irrespective of its total crustal thickness [*Kelemen and Holbrook*, 1995; *Holbrook et al*., 2001; *Korenaga et al*., 2002]. We calculated

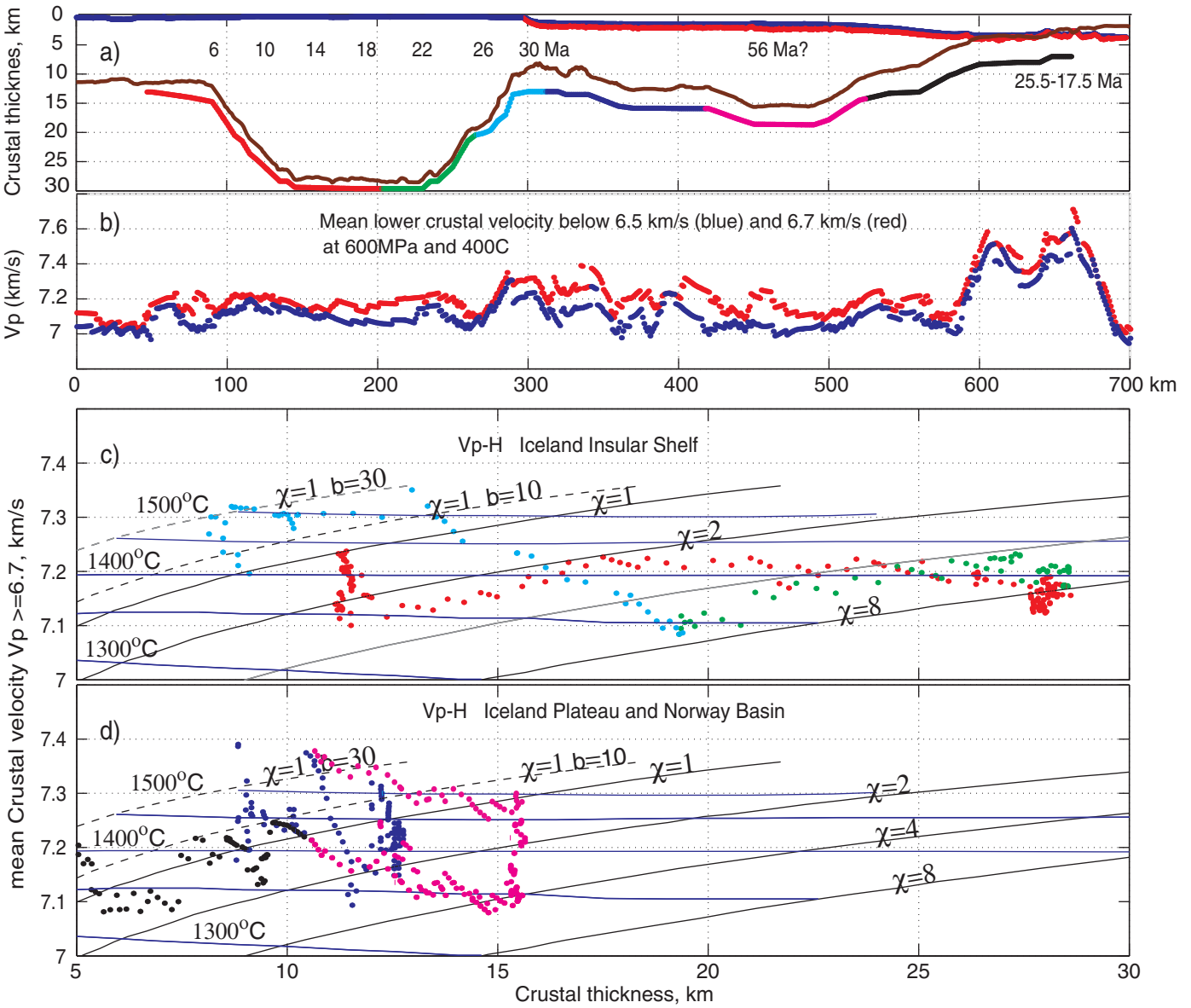

Figure 7. Average lower crustal velocity (Vp) and crustal thickness (H) along KRISE7. (a) Plot of seafloor topography (blue), basement (red), and Moho with colors indicating different regions discussed in text. Brown line shows total crustal thickness (from basement to Moho). Crustal age is based on the NUVEL-1A spreading model [*DeMets et al.*, 1994] with a half-spreading rate of 0.9 cm/yr at 105°, and distance from magnetic anomaly 5 (10 Ma), at 125 km. (b) Average lower crustal velocity along the KRISE7 line, below the 6.5 (blue), and the 6.7 (red) km/s isovelocity contours. Higher-velocity anomalies are associated with narrow (~30 km) lower crustal high-velocity domes. Similar domes characterize both active and extinct central volcanoes of Iceland. (c) and (d) Vp-H across the Iceland Shelf and the Iceland Plateau to the Ægir Ridge, respectively. A 100°C decrease in mantle temperatures is inferred across the Iceland shelf and from the eastern margin of the Iceland Plateau towards the Ægir Ridge. Cessation of spreading at the Ægir Ridge was associated with a marked decrease in inferred mantle temperatures, in line with decreasing supply of partial melt.

average lower crustal seismic velocities in order to assess possible variations in mantle dynamics, from the initiation of spreading within the N-Atlantic to present day rifting, north of Iceland.

An increase in lower crustal velocities at the eastern Iceland Shelf (300 km, cyan region, Figure 7), indicates that the initiation of the KR at 30 Ma was associated with a 100–150° increase in mantle temperatures, reaching a maximum of ~1500°C. Subsequent crustal thickening of 10–15 km and a 0.2 km/s decrease in lower crustal velocities toward Iceland (260–310 km along profile, cyan region in Figure 7), indicates a marked increase in melt flux between 25 and 30 Ma, from plate driven (passive) upwelling to plume driven melt flux (χ) more than four times the surface divergence rate. A decrease in mantle temperatures in the presence of higher melt flux may signify an increase in mantle fertility, possibly due to reworking of older

(oceanic) mantle (and crust) at the initiation of the new spreading center [*Holbrook et al*., 2001; *White et al*., 2008]. Similarly, decreasing lower crustal velocities toward Iceland signify a 100–150°C decreasing mantle temperatures and a gradual decrease in melt flux, since the initiation of the KR (25–200 km, red region in Figure 7). The initiation of the KR thus seems to have been associated with a marked increase in mantle temperatures and melt flux, decreasing to present values at about 10 Ma.

In summary, the crustal structure along this section reflects considerable variations in crustal upwelling and extrusion rates diminishing with time from the initiation of the KR to the present. The overall crustal structure and thickness at the Iceland Shelf is similar to plume-influenced crust in E-Iceland [*Staples et al*., 1997].

4.2. Crustal Evolution of the Iceland Plateau 300–500 km

The Iceland Plateau encompasses crust formed at the western flank of the ÆR prior to the initiation of the KR. The IP is of cryptic age and sits at intermediate depth, close to 2800 m. The eastern IP encompasses crust formed during cessation of spreading at the ÆR, prior to the initiation of the KR, including the former central E-Greenland margin.

4.2.1. Sediments on the Iceland Plateau

The sediment thickness across the western IP is nearly 1 s (∼1000 m, between 300 and 450 km), separated by an unconformity from a ≥100 km wide zone of 1.5 s (1500 m) sediment thickness at the eastern IP margin (Figures 2 and 8). Two prominent intrasedimentary reflectors are visible in this region, at ∼0.2 s across the IP and at ∼0.5 s within the thickest section on the eastern IP margin. The upper reflector coincides with middle Miocene tephra layers (reflector R1 at 223 m, 0.28 s thick) in ODP core 985 [*Jansen et al*., 1996], located on the gentle slope of the eastern IP margin, approximately 75 km north of our profile. A sequence of irregular reflectors overlying R1 can also be traced across the IP, representing younger Miocene ash layers, which have been traced by geochemical analyses to central volcanoes in Eastern Iceland [*Wallrabe-Adams and Werner*, 1999].

The deeper reflector corresponds to reflector R2 of middle-Miocene age at 320 m (0.4 s thickness) depth in hole ODP985, and shallows from ∼0.5 s to ∼0.35 s along our profile. Below R2, the 588 m long ODP985 core penetrated an early-Miocene—late Oligocene sedimentary sequence with more homogeneous and intermittent reflectors [*Jansen et al*., 1996] similar to the character of the KRISE7 seismic reflection section. Basalts drilled at site 350 are considered to have intruded highly altered tuff breccias, overlain by sediments of late Eocene age [*Kharin*, 1976]. Conrad 1978 reflection profiles 207, 208, and 209, further north across the IP (Figure 8) show the overall sediment thickness decreasing westward and northward. A nearly constant sediment thickness of 1.5 s along the eastern IP margin, from the KRISE7 profile toward the Jan Mayen Ridge, marks Paleogene-Eocene sediments deposited within the Norway basin during the opening of the North-Atlantic.

4.2.2. Crustal Structure of the Iceland Plateau and Former Central E-Greenland Margin

The Iceland Plateau is characterized by rough basement. A ∼80 km wide region near the eastern IP margin (∼450 km, between OBS stations 47 and 50) and south of the Jan Mayen Ridge has basement peaks rising up to 600 m, and thicker sediments than adjacent regions. This basement morphology is similar to that of the Kolbeinsey and Reykjanes Ridges and we infer that it was generated by extension and tectonism at an IP extinct rift (discussed below).

Similar to the Iceland Shelf, lateral variations in compressional velocity are prominent across the Iceland Plateau (Figure 6). The average depth to the 5.0 km/s isovelocity contour (layer 2a thickness) is around 2 km (Figure 4), similar to the Iceland-Faeroe Ridge [*Smallwood et al*., 1999]. Total upper crustal thickness (depth to isovelocity contour 6.5 km/s, Layer 2–3 boundary) is 6–8 km. While the upper crust is thickest at the western IP margin, within the region formed at the initiation of spreading at the KR around 26 Ma, the total crustal thickness increases eastward, from 12–13 km at 300–425 km to about 15 km at the IP eastern margin (450–500 km).

Compressional to shear wave velocity ratios (V_P/V_S) have been widely used as a diagnostic tool to determine crustal lithologies and temperatures [*Mjelde et al*. 2002, 2007 and references therein]. Based on converted shear waves on horizontal components of some stations along the KRISE7 profile, we observe crustal V_P/V_S ratio ranging from 1.76 to 1.8 beneath the Iceland Shelf and 1.75 to 1.85 across the Iceland Plateau. These values fall within the 1.74–1.8 range observed along refraction profiles crossing Iceland [*Menke et al*., 1996;

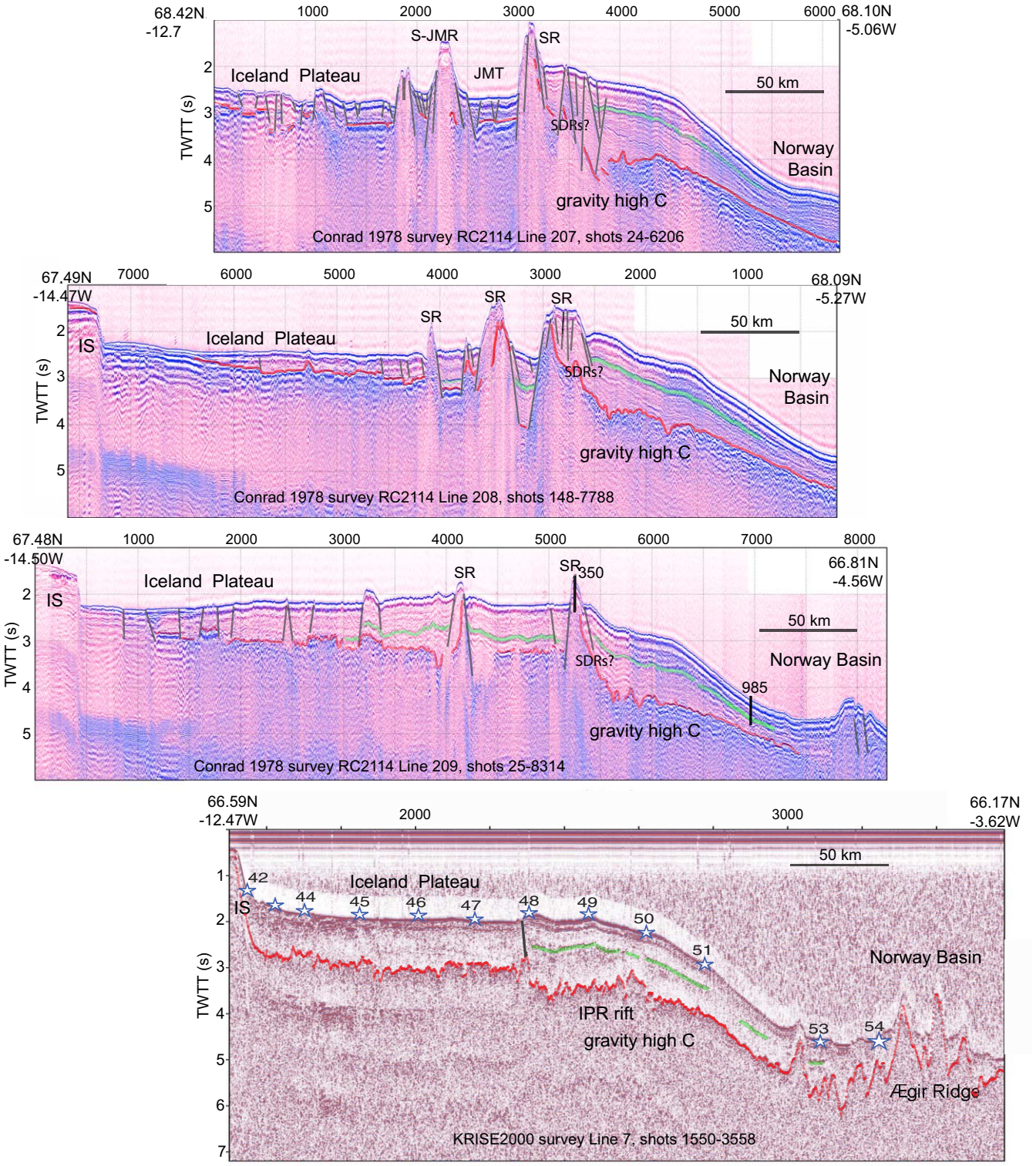

Figure 8. Conrad 1978 reflection profiles 207, 208, and 209 and the eastern section of the KRISE7 profile. Data from the University of Texas Institute for Geophysics, Marine Geoscience Data System. Note prominent internal sediment reflectors, presumably middle Miocene in age (green line) along the eastern margin of the Iceland Plateau, between 450 and 500 km and vertical unconformity west of OBS48, dashed line. DSDP hole 350 (star) penetrated basalts within the easternmost basement ridge.

Staples et al., 1997; *Darbyshire et al*., 1998; *Weir et al*., 2001; *Allen et al*., 2002] and the Iceland-Faeroe Ridge [*Smallwood et al*., 1999]. Although V_P/V_S ratios may theoretically be used to distinguish between felsic (1.71–1.78) and mafic (to 1.84) rocks [*Holbrook et al*., 1992], observed ratios within the lower crust beneath the Jan Mayen Basin (1.75–1.8) [*Mjelde et al*., 2007] fall in the range of oceanic crustal layers 2B and 3 beneath the IP. V_P/V_S ratios may thus be of limited use in distinguishing crustal origin within this region.

Fluid-dynamic models require higher mantle temperatures during initiation of new spreading centers where lower viscosity and small-scale convection contribute to excess melt generation at breakup, followed by steady state plate-driven flow [*Nielsen and Hopper*, 2004]. Alternative models involve sublithospheric convection driven by surface cooling bringing up dense fertile mantle without a thermal anomaly [*Korenaga*, 2004]. The Iceland Plateau is of particular interest with respect to plume versus plate-driven magmatism, mantle potential temperatures, and crustal formation during breakup of the central E-Greenland margin.

Lateral variations in lower crustal velocities beneath the IP are associated with ~50 km wide higher velocity domes at 300–350 km and 380–430 km (dark blue and black region in Figures 7a and 7d). A slight gravity high at 410–460 km (Figures 5a and 5b) corresponds with the eastern dome, whereas thicker upper crust at the Iceland margin may counteract the gravity high of the western dome. Similar lower crustal domes, representing intrusive complexes, characterize both active and extinct central volcanoes in Iceland [*Pálmason*, 1971; *Brandsdóttir et al*., 1997; *Brandsdóttir and Menke*, 2008], the edge of the Iceland Shelf along the Iceland-Faeroe Ridge [*Smallwood et al*., 1999] as well as continental-oceanic boundaries across the N-Atlantic margins [*Korenaga et al*., 2002; *Hopper et al*., 2003; *White and Smith*, 2009]. Lower crustal domes along the Faroe Platform and Hatton margin are made up of lower crustal sills intruded into continental crust during the breakup of the N-Atlantic [*White et al*., 2008; *White and Smith*, 2009]. The 40 km wide lower crustal dome imaged beneath the Hatton margin [*White and Smith*, 2009] is of similar dimensions as the IP and the KR domes. Velocity-crustal thickness (Vp-H) patterns indicate that the domes signify accumulation of intrusive complexes under elevated mantle temperatures at both presently active (KR) and extinct (IP) spreading centers.

Since the initiation of spreading in the N-Atlantic, crustal formation has been asymmetric in the region northeast of Iceland. The crust beneath the IP is 3 km thicker than crust of similar age beneath its conjugate Møre Basin and 4–7 km thicker than 300 km further north, west of the Jan Mayen Basin, where crust considered to have formed at the initiation of the Kolbeinsey Ridge has a thickness of 8.0–9.5 km [*Kodaira et al*., 1998b]. The IP crust is also slightly thicker than normal oceanic crust in the Atlantic [*White*, 1992], with a similar range in primary mantle potential temperatures as between Iceland and MORB [*Slater et al*., 2001; *Herzberg et al*., 2007]. These observations suggest that the IP has been generated by high melt flux under influence of the Iceland plume.

A ~45 km wide region, at the eastern margin of the IP, beneath the thickest sediment cover (Figure 8) represents the former central E-Greenland margin (R2, within purple region in Figure 7). This section of the profile has a lower crustal velocity ranging from 7.1 to 7.3 km/s and a crustal thickness of 15 km, which is higher than the 11 km modeled at its conjugate Møre margin [*Breivik et al*., 2006] but significantly lower than the ~23.5 km modeled along the Vøring margin [*Mjelde et al*., 2005]. Igneous crustal thickness further north, along the eastern margin of the Jan Mayen microcontinent varies from 7–9 km in the north to 12–14 km in the south [*Breivik et al*., 2012]. Igneous crust accreted to the former central E-Greenland is thus significantly thinner than at the SE-Greenland margin on the SIGMA III profile (~18 km) [*Hopper et al*., 2003] and its conjugate margin, the Hatton Bank (18–23 km) [*White and Smith*, 2009]. Based on these observations, it is clear that during early Eocene breakup magmatism varied substantially, or was preferentially channeled, along both margins of the N-Atlantic.

A comparison of lower crustal velocities on each side of the former central E-Greenland margin is of interest as they represent regions of initial oceanic crustal formation associated with rifting at the Ægir Ridge (R1, Figure 7) and oceanic crust generated within the IP rift (R3, Figure 7) during cessation of spreading within the southern Norway Basin and prior to the formation of KR. A similar degree of crustal thinning following spreading center initiation is observed in both regions. However, lower crustal velocities associated with the IP rift are up to 0.2 km/s higher, indicating the activation of an overlapping spreading center was prompted by a significant increase in potential mantle temperature of up to 200°, which surprisingly, is coincident with a decrease in mantle flux from four to less than two times the surface divergence rate.

Based on channeled plume models, it is likely that declining spreading rates within the southern Norway basin and formation of an overlapping spreading center (OSC) were associated with eastward channeling from the Iceland plume.

In summary, slivers of continental crust sheared off the central E-Greenland margin with the Jan Mayen Ridge are not detected along the KRISE7 profile. Since the average crustal velocities are typical of oceanic crust, any continental slivers in this region must have been severely extended and intruded. Although lack of continuous magnetic anomalies (Figure 1b) adds to uncertainties in the evolutionary history of the crust in this region, the lower crust on both sides of the former central E-Greenland margin is oceanic in character, created under mantle instabilities associated with plate boundary initiation.

4.3. Crustal Structure of the Norway Basin and the Ægir Ridge, 500–700 km

The Norway Basin has an upper/lower crustal ratio of 1:1 with an upper crustal thickness decreasing eastwards from 4–5 to 2–3 km at the Ægir Ridge. No Moho reflections are observed along the easternmost 100 km of the KRISE7 profile, possibly because of rough basement topography. Based on crustal thickness inferred from the depth of the 7.4 km/s isovelocity contour along the ÆR, the overall crustal thickness decreases from 8–10 km at the eastern margin of the IP (500–600 km) to 4–5 km at the ÆR. The ÆR crustal thickness is slightly less than the 5.5–6.5 km thickness observed by *Grevemeyer et al*. [1997], near our profile. However, our thickness at the ÆR is similar to the 4–5.5 km crustal thickness at the extinct Labrador spreading center, perhaps reflecting values typical of a decreasing supply of partial melt preceding extinction [*Osler and Louden*, 1995]. The 70–80 km wide ÆR is characterized by broad basement peaks that rise up to 1000 m above the seafloor. Light REE depleted tholeiitic rocks [*Schilling*, 1976] from DSDP hole 337 at the SE flank of the ÆR (Figure 1), dated by separate laboratories at 17.5 and 25.5 Ma [*Kharin et al*., 1976], indicate that at axial highs adjacent to the rift valley, younger lavas were extruded onto substantially older, early-middle Oligocene (32–38 Ma) sediments.

Although a thick sediment cover drapes the ÆR axis, its general bathymetry [*Jung and Vogt*, 1997], magnetics, and gravity [*Greenhalgh and Kusznir*, 2007] indicate that the cessation of spreading was associated with more elevated and continuous rift mountains and deepening of the central rift valley southward. The mean velocity of crust generated at the ÆR increases as the crustal thickness decreases from 10 to 5 km. An increase in lower crustal velocity across the western flank of the ÆR (580–680 km) is associated with a broad ($>$100 km) region of markedly thinner crust. The Vp-H diagram indicates a 100–150°C decrease in mantle temperatures across the western Norway Basin from the eastern margin of the Iceland Plateau towards the ÆR (black region, Figure 7). We infer that cessation of spreading at the ÆR was associated with a marked decrease in mantle temperatures $>$100°C within a near plate-driven (passive) upwelling regime ($\chi \sim 1$) in line with decreasing supply of partial melt toward the dying Ægir Ridge axis.

5. Discussion

5.1. Rifting at the Former Central E-Greenland Margin and Iceland Plateau

The opening of the N-Atlantic was accompanied by excessive magmatism marked by thickened igneous crust and extensive subaerial volcanism, presently marked by seaward dipping reflectors (SDRs) at the central E-Greenland margin [*Larsen and Jakobsdóttir*, 1988; *Larsen and Saunders*, 1998], the eastern margin of the Jan Mayen microcontinent (JMMC) [*Gernigon et al*., 2012], the Vøring Plateau [*Mutter and Zehnder*, 1988; *Mutter et al*., 1988; *Mjelde et al*., 2005], the Møre margin [*Grunnaleite and Gabrielsen*, 1995; *Gernigon et al*., 2012], and Hatton Bank [*White and Smith*, 2009 and references therein].

Broad (50–100 km), well-defined gravity highs associated with early-breakup magmatism are present within the continental-ocean boundary (COB) zones along outer shelfs of N-Atlantic margins (Figure 9a). Gravity high C [*Talwani and Eldholm*, 1977] along the eastern margin of the IP, is of similar origin as highs along the COB of the conjugate Møre margin which have been associated with "embryonic spreading cells" and "magnetic clusters" [*Gernigon et al*., 2012] along the $\sim$100 km wide COB, spanning magnetic anomalies C24A, C24B, and the inner SDRs, showing that the Møre margin was subjected to an oblique sheared stress regime at the onset of breakup. Furthermore, recently acquired high-resolution seismic reflection profiles across the conjugate JMMC have illuminated rifted and tilted fault blocks, interspersed between regions of oceanic crust (including SDRs) formed by seafloor spreading [*Gaina et al*., 2009; *Peron-Pinvidic et al*., 2012].

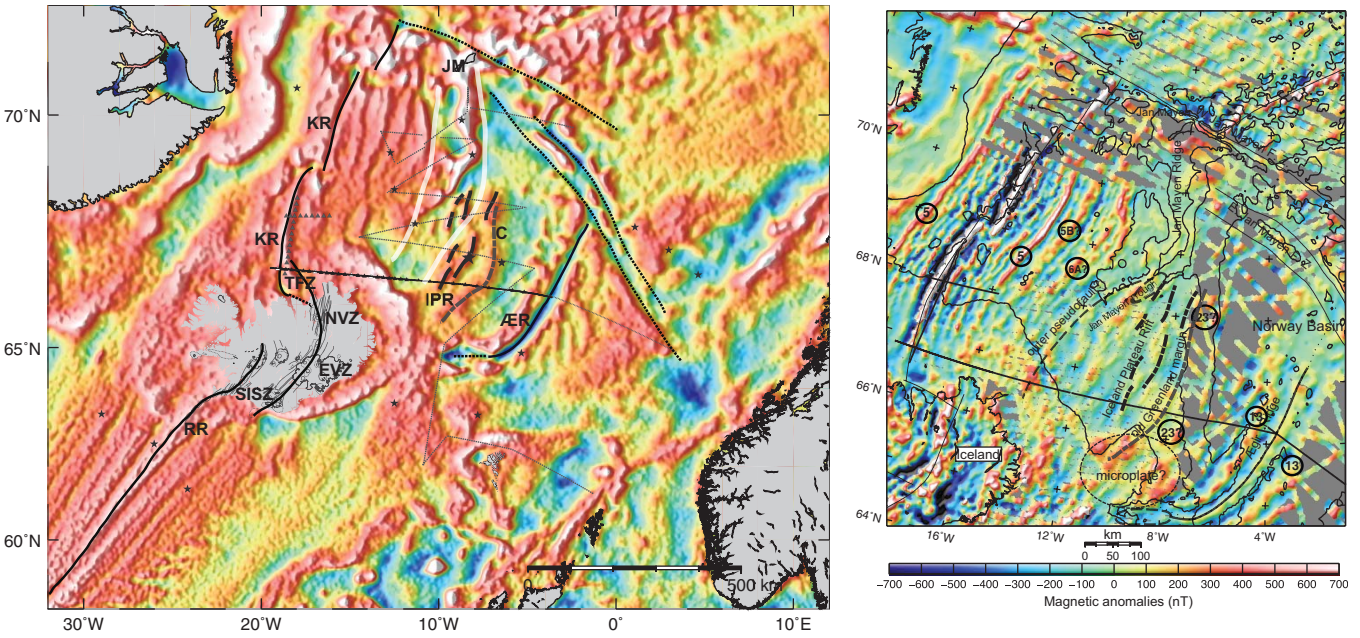

Figure 9. Present and extinct plate boundaries within the Iceland region, derived from gravity and refraction-reflection data, plotted on a free-air ERS 1 satellite gravity map [*Sandwell and Smith*, 1997], illuminated from NW (a) and magnetic anomaly map (b). The Iceland Plateau Rift (IPR) formed a branched rift axis that overlapped the dying Ægir Ridge and generated thickened crust due to the influence of the Iceland plume. Dashed lines indicate major transform zones. DSDP and IODP core sites are marked with stars. The IPR lies along basement ridges previously identified from seismic reflection and gravity data by the Conrad 1978 and older surveys [*Talwani and Eldholm*, 1977]. White lines mark the Jan Mayen (JM) Ridge area as defined by *Talwani and Eldholm* [1977]. Figure 9b Circled numbers refer to magnetic anomalies. Areas devoid of data are gray. Magnetic anomaly 23 follows the eastern margin of gravity ridge C (gray-dashed line) which represents the former central E-Greenland margin.

Talwani and Eldholm [1977] were the first to theorize complicated sea-floor spreading associated with fan-shaped spreading of the Ægir Ridge by acknowledging that the "eastern ridges were formed by sea-floor spreading in complementary fashion to fan-shaped lineations of Norway Basin," and placing the second rift axis between the Jan Mayen Ridge and their gravity lineation C (Figure 9). *Talwani and Eldholm* [1977] also suggested that "a number of spreading centers interspersed between areas of continental crust could have existed in this region." In order to explain the fan-shaped anomaly pattern around the Ægir Ridge, a complementary spreading axis with rift propagation in the opposite direction is required, forming an OSC west of the Ægir Ridge axis, within the Iceland Plateau.

Based on our compilation of the KRISE7 crustal model with other geophysical data, we are able to constrain how the cessation of spreading within the Norway Basin was associated with rift reactivation along the former suture zone of the central E-Greenland margin (Figure 9). The KRISE7 refraction profile reveals the location and structure of several immature spreading axes beneath the IP region including the IP rift, whereas the reflection data illuminates a sediment unconformity, pinpointing the location of the former central E-Greenland margin. The IP rift axis does not have a distinctive topographic expression along the KRISE7 profile. However, the relatively small basement peaks become larger to the north (Figure 8).

The eastern Iceland Plateau was the locus of an extinct spreading center, which was segmented and overlapped the Ægir Ridge by about 300 km. Lower crustal domes and corresponding gravity highs across the Iceland Plateau mark the location of the extinct rift axis. Spreading on the Iceland Plateau rift occurred simultaneous with that on the Ægir Ridge and prior to 26 Ma, when the Kolbeinsey Ridge initiated to the west. We find thick crust (12–15 km) formed at the Iceland Plateau Rift under active upwelling conditions (normal lower crustal velocities) and attribute this to the influence of the Iceland plume. We infer that this influence, together with the overlapping geometry of the Ægir and Iceland Plateau ridges, led to progressive south to north abandonment of spreading on the Ægir Ridge. Iceland Plateau rift propagated along the continent-ocean transition at the former central E-Greenland margin, perhaps associated with the formation of the Jan Mayen Ridge. The northward propagating Iceland Plateau Rift underlies a region with diffuse magnetic anomalies (Figure 9b). The western part of this region may mark the western extent of the

propagator as an outer pseudofault into the Jan Mayen Trough. The southern part of the diffuse magnetic region may represent a microplate trapped between the two asymmetric rift axes and a transform zone at the southern tip of the Ægir Ridge.

Instead of creating a well-developed rift segment the IP rift became confined to interspersed magmatic segments, en echelon along a relatively broad extensional zone (100–150 km) just west of the former central E-Greenland margin. Magma propagated northwards along the IP rift and was intruded into the overlying sedimentary sequence forming parallel ridges south of the Jan Mayan microcontinent. Gravity ridge C, which protrudes from the northeastern Iceland Shelf (Figure 9), follows the 1500 m depth contour, turning northward and crossing the KRISE7 line just west of OBS 51 (Figure 8), runs semiparallel to the basement ridges [*Talwani and Eldholm*, 1977]. No major transfer zones offset gravity high C. This region, defined as region 3 by *Talwani and Udintsev* [1976] has a controversial origin, considered by *Talwani and Eldholm* [1977] to represent oceanic crust generated by spreading at the southern Ægir Ridge, whereas *Gairaud et al*. [1978] considered it to be a part of the old Greenland margin. Our model of the formation of the IP rift prior to the westward rift jump that generated the KR, is in agreement with *Kuvaas and Kodaira* [1997] and *Mjelde et al*. [2008] who argued that continental stretching between central E-Greenland and Jan Mayen Ridge was active for at least 20 Myr before the initiation of the Kolbeinsey Ridge.

Early Eocene breakup basalts around the N-Atlantic were created under the influence of an ancestral Iceland Plume [*Schilling*, 1976]. Light-rare-earth elements (REE) analyses of basalts sampled from DSDP cores within and around the Norway Basin (Figure 1) indicate that the plume-influence has been locally channeled throughout the N-Atlantic region since early Eocene. Basalt specimens from DSDP350 on the easternmost IP ridge (Figures 8 and 9) have similarly enriched light RE composition as DSDP sites 342 (Middle Eocene) and 343 on the Vøring Plateau, the lower Faeroes Plateau basalt series and East Greenland Plateau basalts, indicating that they are plume-derived [*Schilling*, 1976]. In contrast, tholeiite sampled from DSDP site 337, near the Ægir axis (Figure 1), had light RE-depleted patterns typical of normal mid-ocean ridge segments [*Schilling*, 1976]. The DSDP350 basalts (three samples) have radiometric ages ranging between 33.5 and 50 Ma and were intruded into highly altered tuff breccias and overlain by sediments of tentative late Eocene (43–38 Ma) age [*Kharin et al*., 1976]. Although the potassium-argon age determinations are not well constrained, intrusions into late Eocene sediments indicate that the basalts were erupted/intruded within the IP rift under the influence of the Iceland plume but that this influence did not extend to the Ægir ridge at 17 or 28 Ma or the central KR (site DSDP 348, 17, or 28 Ma), (Figure 1) [*Kharin*, 1976; *Schilling*, 1976]. Furthermore, *Kharin et al*. [1976] state that "an age of 41.2$\pm$1.0 m.y. would be in agreement with an extrusion or intrusion of the basalt in the youngermost Eocene before the extinction of the axis in the Norwegian Sea, when the Jan-Mayen Ridge and its morphological extension to the south was part of the Greenland continent or its shelf area."

Large magnetic clusters on the southern IP and eastern insular shelf of Iceland (Figure 1b) represent embryonic spreading cells, i.e., extinct central volcanoes, akin to those now active within the Neovolcanic Zones in Iceland [*Kristjansson et al*., 1977]. Assuming that these volcanic systems were plume-influenced, they would have been more productive than those along the rift axis. Complex central volcanoes could thus have represented the western arm (IP rift) of an overlapping spreading center extending from the eastern insular shelf of Iceland north and parallel to the Ægir Ridge.

5.2. Rifting at the Kolbeinsey Ridge and N-Iceland Shelf

Based on compilations of thickened oceanic crust along the N-Atlantic margins and across the N-Atlantic, via the Greenland-Iceland-Faeroe Ridge, plume-influence within the N-Atlantic has been both spatially and temporally episodic [*Eldholm and Grue*, 1994], indicating channeled mantle flow along breakup zones and rift systems, as supported by geodynamic models [*Ito et al*., 2003]. The influx of material from the Iceland plume has generated 20–40 km thick crust beneath Iceland [*Brandsdóttir and Menke*, 2008], $\sim$30 km beneath the Iceland-Greenland [*Hopper et al*., 2003] and Iceland-Faeroe Ridges [*White et al*., 2008], and thickened crust along the spreading centers north [*Hooft et al*., 2006] and south [*Weir et al*., 2001] of Iceland. Seismic, bathymetric, and geochemical data indicate that at present plume material is preferentially diverted southward along the Reykjanes Ridge where crustal thickness is $\sim$2 km greater than along the KR [*Mertz et al*., 1991; *Sandwell and Smith*, 1997; *Weir et al*., 2001; *Hooft et al*., 2006].

The initiation of the Kolbeinsey Ridge is recorded in thickened oceanic crust (up to 30 km) at the eastern Iceland Shelf. Magmatism at the newly formed Kolbeinsey Ridge was associated with unusual large

amounts of extrusive volcanism as recorded by an extremely thick (4–6 km) upper crustal layer (2A, >5 km/s) in this region (Figure 4). Based on bathymetry and seismic data [*Brandsdóttir and Menke*, 2008; *Smallwood et al*., 1999], similar crustal structure is observed along other parts of the Iceland Shelf and along the southward propagating rift in Iceland, indicating that similar processes govern the formation and initial development of a plume-influenced rift. A decrease in crustal thickness toward the current plate boundary from nearly 30 km on the eastern shelf to 9–12 km at the Kolbeinsey Ridge axis [*Hooft et al*., 2006] reflects a significant decrease in melt production at this ridge segment from 22 Ma to the present.

Although the material properties of the thickened lower crust beneath the Iceland platform remain an enigma, seismic velocities of ≥7 km/s within a 10–12 km thick lower crustal layer signify oceanic crustal origin. Recent, high-resolution seismic profiles show that basaltic melt is intruded into the lower continental crust as sills or dykes, rather than ponding at the base of the crust in an underplated material [*White et al*., 2008].

Seismic refraction profiles across the divergent plate boundary in Iceland have revealed steep Moho topography, with marginal dips ranging from 6 to 12° [*Brandsdóttir and Menke*, 2008]. A decrease in crustal thickness of 5 km to the west and 10 km to the east from the center of the NVZ, over a distance of ∼25 and ∼50 km, is associated with a Moho dip of 5°. Similar dips occur offshore northern Iceland where the crust thickens from 12 km along the southernmost Kolbeinsey Ridge to 25 km on land [*Hooft et al*., 2006; *Brandsdóttir and Menke*, 2008]. We observe Moho dips of 3–4° along the Iceland Shelf where crustal thinning of ∼14 km occurs over a distance of ∼50 km (Figure 4). Based on laboratory experiments indicating that oceanic lower crustal gabbros undergo ductile deformation at temperatures above 800°C [*Hirth et al*., 1998], one might expect that Moho topography would tend to collapse over time. Instead the Moho topography may be sustained by older and cooler lower crustal segments flanking younger (< 7Ma) rift zones.

6. Conclusions

Spreading north of Iceland has been complicated with the locus of rifting repeatedly relocating westward as the Iceland plume approached the Mid-Atlantic Ridge from the west. The 700 km long KRISE7 seismic refraction/reflection and gravity profile, straddles 66.5°N and crosses the three physiographic provinces that characterize this region: the Iceland Shelf, Iceland Plateau, and Norway Basin. On the basis of crustal thickness and velocity structure, combined with older seismic reflection profiles and drill cores, we conclude that these provinces correspond to three individual spreading rifts that were active at different time periods.

The deep, fan-shaped Norway basin was formed during initial opening of the Atlantic by spreading at the now extinct Ægir Ridge. The oldest crust in the western Norway Basin has thickness 8–10 km and this thins to 4–5 km at the Ægir Ridge reflecting the progressive abandonment of spreading at this rift axis.

We propose that the eastern Iceland Plateau was the locus of an extinct spreading center, which was segmented and overlapped the Ægir Ridge by 300 km. Lower crustal domes and corresponding gravity highs across the Iceland Plateau mark the location of the extinct rift axis. Spreading on the Iceland Plateau rift occurred simultaneously with that on the Ægir Ridge prior to 26 Ma, when the Kolbeinsey Ridge was initiated by a westward rift jump. The crust at the IPR is thicker (12–15 km) than that at the conjugate ÆR and formed under active upwelling conditions (normal lower crustal velocities), which we attribute to the influence of the Iceland plume. The overlapping geometry of the Ægir and Iceland Plateau ridges, led to progressive south to north abandonment of spreading on the Ægir Ridge. We also suggest that the Iceland Plateau rift formed by rifting along the continent-ocean transition at the former central E-Greenland margin, perhaps associated with the formation of the Jan Mayen Ridge.

Rifting at the Kolbeinsey Ridge in the last 26 Ma formed the shallowest physiographic province, the Iceland Shelf. Initiation of the Kolbeinsey Ridge is recorded in very thick crust (24–28 km) at the eastern Iceland Shelf. Extensive melting beneath this new spreading axis was due to significant increase in melt flux (active, plume-driven upwelling), generating very thick crust with normal velocities under fairly stable thermal conditions. This greater plume influence caused the spreading axis to jump from the Iceland Plateau—Ægir rift system to the new Kolbeinsey ridge. We infer that this is due to enhanced buoyant upwelling associated

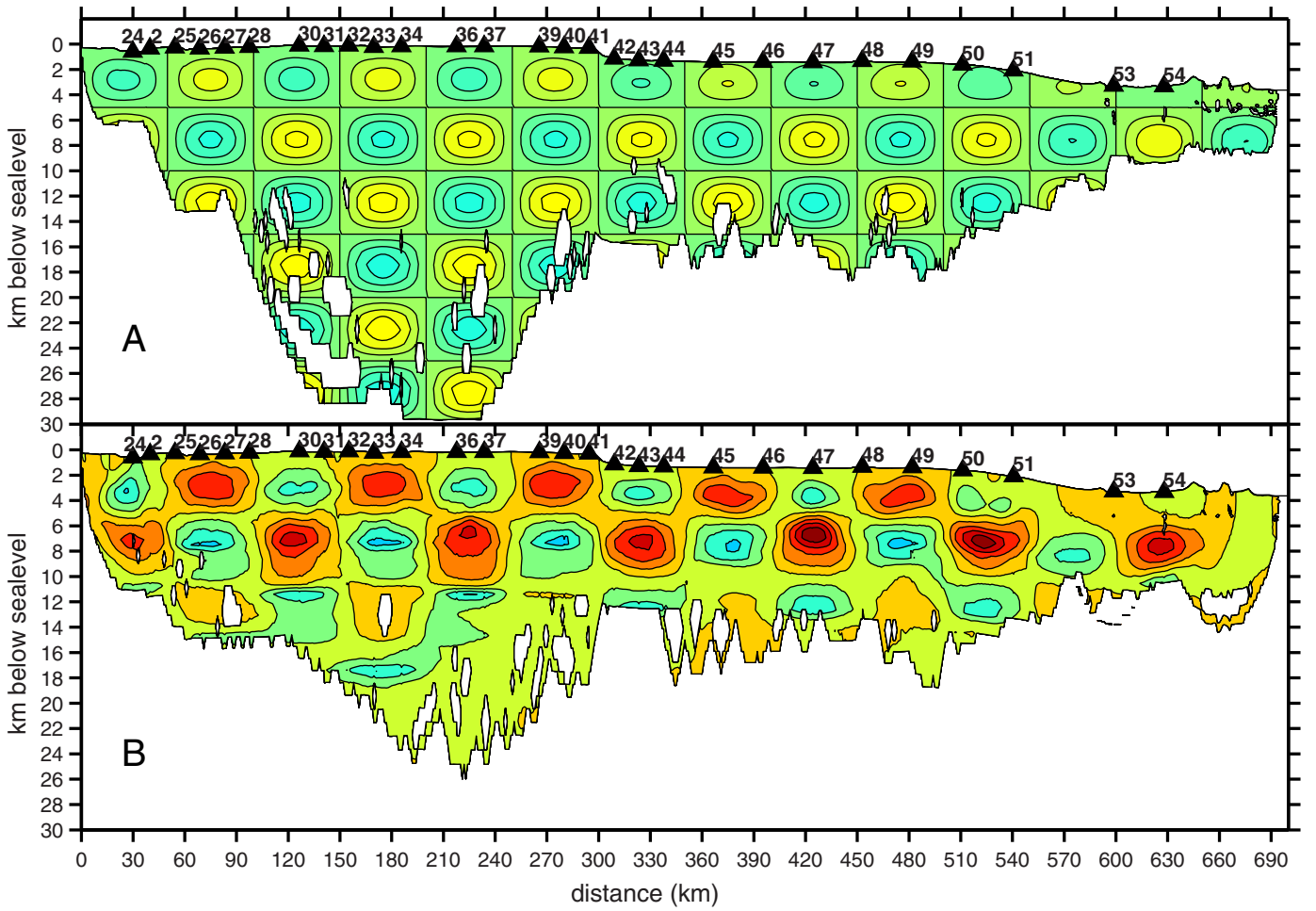

Figure A1. (a) Initial model: positive and negative checkerboard pattern velocity anomalies of ±0.75 km/s with 50 km horizontal and 5 km vertical wavelengths. (b)Anomalies recovered reflect high model resolution within the uppermost 10 km.

with the Iceland plume. Magmatism at the new Kolbeinsey Ridge was also associated with unusual large amounts of extrusive volcanism as recorded by an extremely thick (6 km) layer of low velocities in this region. This crustal structure appears to be associated with the development of a plume-influenced rift and is found at the southward propagating rift in Iceland as well as at other parts of the Iceland Shelf edge.

Since its initiation, the melt supply to the Kolbeinsey Ridge has halved; crustal thickness decreases westward from nearly 30 km near the eastern shelf edge to 12–14 km at the Kolbeinsey Ridge axis. This reduction in melt supply was accompanied by a decrease in active mantle upwelling and a transition to a more usual ratio of extrusive to intrusive volcanism.

As the Iceland plume approached the Mid-Atlantic ridge from the west, three separate spreading centers formed—each progressively further west. We envision that magma from the plume generated new zones of weakness at the continent-ocean boundary and thus formed new spreading rifts. We find thicker crust and a greater plume influence as each successive spreading center initiated. However, thinning crust suggests that plume influence at the Kolbeinsey Ridge has declined since 20 Ma, perhaps as the Iceland plume moved to the southeast of this region.

An outstanding question is why the spreading north and south of Iceland has responded so differently to the approaching Iceland plume. In contrast to the region north of Iceland that experienced successive rift jumps, spreading at the Reykjanes ridge to the south occurred continuously since the opening of the Atlantic. However, spreading on the Reykjanes Ridge did transition from a segmented axis oriented normal to the spreading direction to a continuous axis rotated oblique to the spreading direction at ~37–40 Ma

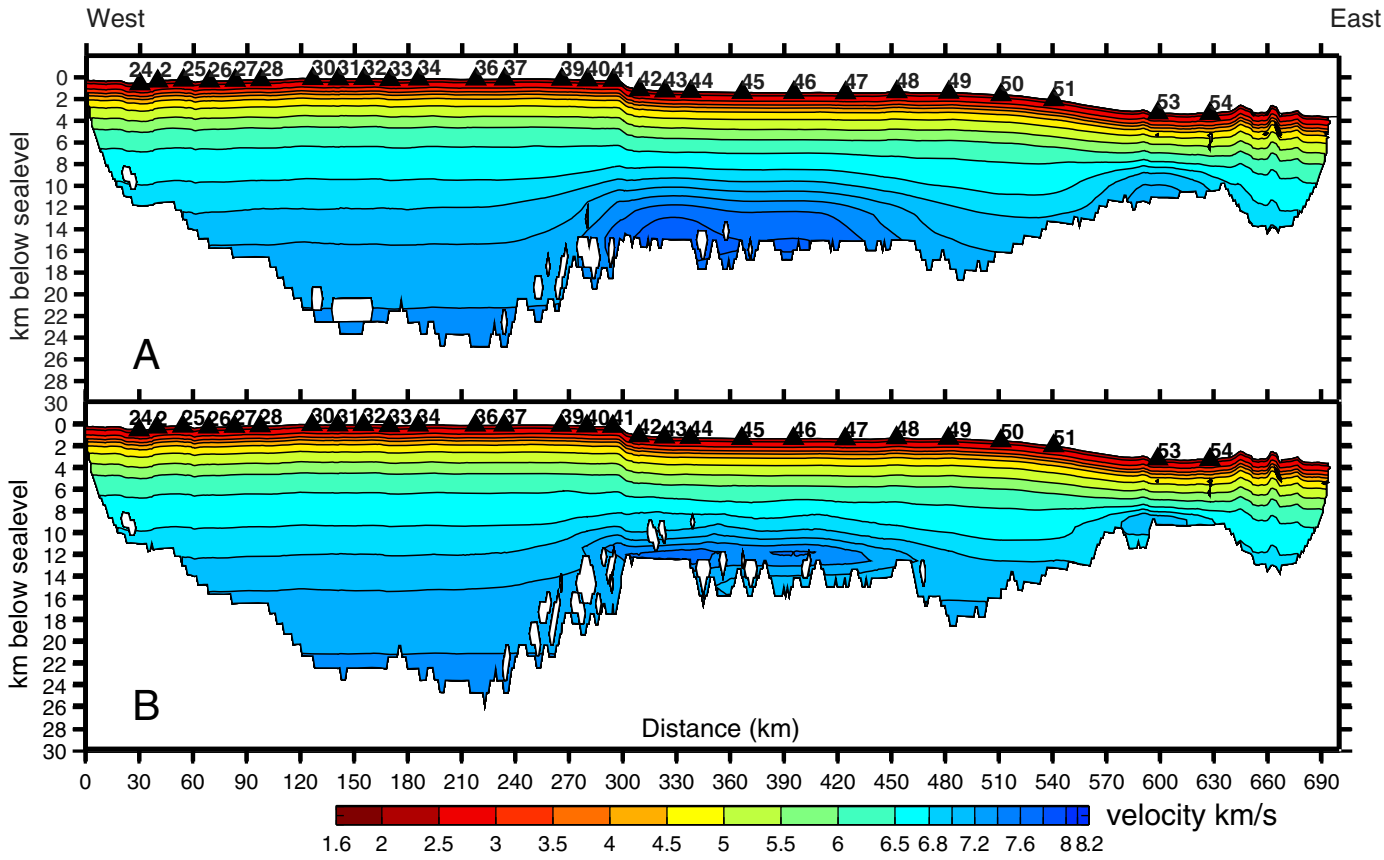

Figure A2. Lower crustal checkerboard resolution test: 5% anomalies with 200 and 100 km horizontal wavelength and 10 km vertical wavelength superimposed on the mean velocity-depth model. Velocity perturbations of this size are fairly well recovered.

(between magnetic anomalies 17 and 18) [*Jones et al*., 2002], indicating enhanced plume influence along the ridge in late Eocene.

Appendix A: Model Resolution Tests

To investigate the reliability of the final crustal model, we use several approaches: (1) investigate the resolution of the model, (2) explore the dependence of the recovered structure on the starting model and inversion parameters, (3) invert synthetic checkerboard-pattern crustal velocity anomalies, and (4) test the resolution of specific observed structures. The resolution of the model can be approximated by the DWS and is discussed in the main body of text.

We performed tests to resolve the overall resolution of our model and in particular the two-dimensional model ability to resolve large-scale features in the lower crust within the Iceland Plateau. We placed positive and negative velocity anomalies of $\pm$0.75 km/s with 50 km horizontal and 5 km vertical wavelengths superimposed on the mean velocity-depth model, in a checkerboard pattern within the profile (Figure A1). The model was filtered to smooth the edges of the anomalies and prevent ray loss. We then calculated travel times for rays passing through the model with the same source-receiver configuration as that used in our experiment. Starting with the best-fit 1D model, we ran five iterations to recover the checkerboard velocity anomaly pattern. The upper crustal model is best constrained owing to the dense coverage of refracted rays down to 12–14 km depth beneath the Iceland Shelf and Iceland Plateau. The checkerboard pattern is best recovered by the inversion at this depth but also fairly well constrained down to 22 km depth. Our lower crustal resolution tests, on the scale of 100 km and 200 km horizontal wavelength and 10 km vertical wavelength, show that the high-velocity anomalies at the base of the crust are fairly well recovered (Figure A2). The exploration of DWS, inversion parameters, and checkerboard tests all show that the resolution of the crustal model depends primarily on the instrument spacing and the ray coverage.

Acknowledgments

The success of this experiment was due partly to the fair weather, but mainly to the professionalism and smooth interaction of the crews of R/V Håkon Mosby and the Icelandic Coast Guard Cutter Ægir, the University of Bergen air gun crew, and the University of Hokkaido OBS crew. We thank Hideki Shimamura, Tomoki Watanabe, Tadashi Yamashina, Testsuo Takanami, Andrew Barclay, Øystein Aanensen, and Asbjørn Breivik for their valuable contribution to the planning and executing of this survey. KRISE was funded by the National Science Foundations of USA (NSF-OCE-9911243) and Iceland, and the Universities of Hokkaido, Bergen and Iceland. The data for this paper are available upon request, contact bryndis@hi.is. We appreciate the use of the Upicker program provided by William Wilcock at the University of Washington and the TOMO2d joint refraction and reflection travel-time tomography software by Jun Korenaga, Yale University. The GMT software [*Wessel and Smith*, 1991] was used to generate most figures. We thank Asbjørn Breivik for providing magnetic and gravity maps, Leó Kristjánsson for supplying rare reprints of scientific papers from the 1970s and the University of Texas Institute for Geophysics, Marine Geoscience Data System (Joyce Alsop, http://www.ig.utexas.edu/sdc/) for providing reflection data from the 1978 R/V Robert D. Conrad Cruise R2114, led by Peter Buhl and John B. Diebold (NSF 7805733). Comments by John R. Hopper and an anonymous reviewer helped improve the manuscript.

References

Allen, R. M., et al. (2002), Plume driven plumbing and crustal formation in Iceland, *J. Geophys. Res.*, *107*(B8), doi:10.1029/2001JB000584.

Bott, M. (1971), The deep structure of the Iceland-Faeroe Ridge, *Mar. Geophys. Res.*, *1*, 328–351.

Bott, M. (1985), Plate tectonic evolution of the Icelandic transverse ridge and adjacent regions, *J. Geophys. Res.*, *90*, 9953–9960.

Brandsdóttir, B., and W. H. Menke (2008), The seismic structure of Iceland, *Jökull*, *58*, 17–35.

Brandsdóttir, B., W. Menke, P. Einarsson, R. S. White, and R. K. Staples (1997), Færoe-Iceland Ridge Experiment 2. Crustal structure of the Krafla central volcano, *J. Geophys. Res.*, *102*, 7867–7886.

Breivik, A. J., R. Mjelde, J. I. Faleide, and Y. Murai (2006), Rates of continental breakup magmatism and seafloor spreading in the Norway Basin-Iceland plume interaction, *J. Geophys. Res.*, *111*, B07102, doi:10.1029/2005JB004004.

Breivik, A. J., R. Mjelde, J. I. Faleide, and Y. Murai (2012), The eastern Jan Mayen microcontinent volcanic margin, *Geophys. J. Int.*, *188*, 798–818, doi:10.1111/j.1365-246X.2011.05307.x.

Carlson, R. L., and G. S. Raskin (1984), Density of the ocean crust, *Nature*, *311*, 555–558.

Darbyshire, F., I. Th. Bjarnason, R. S. White, and Ó. G. Flóvenz (1998), Crustal structure above the Iceland mantle plume imaged by the ICEMELT refraction profile, *J. Geophys. Res.*, *135*, 1131–1149.

DeMets, C., R. G. Gordon, D. F. Argus, and S. Stein (1994), Effect of recent revisions to the geomagnetic reversal time scale on estimates of current plate motions, *Geophys. Res. Lett.*, *21*, 2191–2194.

Du, Z., and G. R. Foulger (2001), Variations in the crustal structure across central Iceland, *Geophys. J. Int.*, *145*, 246–264.

Du, Z., et al. (2002), Crustal structure beneath western and eastern Iceland from surface waves and receiver functions, *Geophys. J. Int.*, *149*, 349–363.

Einarsson, P., and K. Saemundsson (1987), Earthquake epicenters 1982–1985 and volcanic systems in Iceland, separate map accompanying the book (map), in *I hlutarins edli: Festschrift for Thorbjörn Sigurgeirsson*, edited by Th. Sigfússon, Menningarsjódur, Reykjavík.

Eldholm, O., and C. C. Windisch (1974), The sediment distribution in the Norwegian-Greenland Sea, *Geol. Soc. Am. Bull.*, *85*, 1661–1676.

Eldholm, O., and K. Grue (1994), North Atlantic volcanic margins: Dimensions and production rates, *J. Geophys. Res.*, *99*, 2955–2968.

Eldholm, O., A. M. Karasik, and P. A. Reksnes (1990), The North American plate boundary, in *The Geology of North America, vol. L, The Arctic Ocean Region*, edited by L. J. A. Grantz and J. F. Sweeney, pp. 171–185, Geol. Soc. Am., Boulder, Colo.

Fedorova, T., W.R. Jacoby, and H. Wallner (2005), Crust-mantle transition and Moho model for Iceland and surroundings from seismic, topography, and gravity data, *Tectonophysics*, *396*, 119–140.

Flóvenz, Ó. G., and K. Gunnarsson (1991), Seismic crustal structure in Iceland and surrounding area. *Tectonophysics*, *189*, 1–17.

Foulger, G. R. (2006), Older crust underlies Iceland, *Geophys. J. Int.*, *165*, 672–676, doi:10.1111/j.1365-246X.2006.02941.x.

Furmall, A. V., (2010), Melt production and ridge geometry over the past 10 Myr on the southern Kolbeinsey Ridge, Iceland, MSc thesis, pp. 107, Univ. of Oregon, Eugene, Oregon, USA.

Gaina, C., L. Gernigon, and P. Ball (2009), Palaeocene: Recent plate boundaries in the NE Atlantic and the formation of the Jan Mayen microcontinent, *J. Geol. Soc. London*, *166*, 601–616, doi:10.1144/0016-76492008-112.

Gairaud, H., G. Jacquart, F. Aubertin, and P. Beuzart (1978), The Jan Mayen Ridge synthesis of geological knowledge and new data, *Oceanol. Acta*, *1*, 335–358.

Gernigon, L., C. Gaina, O. Olesen, P. J. Ball, G. Pron-Pinvidic, and T. Yamasaki (2012), The Norway Basin revisited: From continental breakup to spreading ridge extinction, *Mar. Pet. Geol.*, *35*, 1–19, doi:10.1016/j.marpetgeo.2012.02.015.

Gradstein, F. M., J. G. Ogg, M. D. Schmitz, and G. M. Ogg (2012), *The Geologic Time Scale 2012*, vol. 2, 1144 pp., Elsevier, Oxford, U. K.

Greenhalgh, E. E., and N. J. Kusznir (2007), Evidence for thin oceanic crust on the extinct Aegir Ridge, Norwegian Basin, NE Atlantic derived from satellite gravity inversion, *Geophys. Res. Lett.*, *34*, L06305, doi:10.1029/2007GL029440.

Grevemeyer, I., W. Weigel, R. B. Whitmarsh, F. Avedik, and G. A. Dehghani (1997), The Aegir rift: Crustal structure of an extinct spreading axis, *Mar. Geophys. Res.*, *19*, 1–23.

Grønlie, G., M. Chapman, and M. Talwani (1979), Jan Mayen Ridge and Iceland Plateau: Origin and evolution, *Norsk Polarinstitutt Skrifter*, *170*, 25–47.

Grunnaleite, I., and R. H. Gabrielsen (1995), Structure of the Møre Basin, mid-Norway continental margin, *Tectonophysics*, *252*, 221–251.

Herzberg, C., P. D. Asimow, N. Arndt, Y. Niu, C. M. Lesher, J. G. Fitton, M. J. Cheadle, and A. D. Saunders (2007), Temperatures in ambient mantle and plumes: Constraints from basalts, picrites, and komatiites, *Geochem. Geophys. Geosyst.*, *8*, Q02006, doi:10.1029/2006GC001390.

Hirth, G., J. Escartin, and J. Lin (1998), The rheology of the lower oceanic crust; implications for lithospheric deformation at mid-ocean ridges, in *Faulting and Magmatism at Mid-ocean Ridges, Geophys. Monogr. Ser., 106*, edited by R. W. Buck et al., pp. 291–303, AGU, Washington, D. C.

Holbrook W. S., W. D. Mooney, and N. J. Christensen (1992), Seismic velocity structure of the deep continental crust, in *Continental Lower Crust*, edited by D. Fountain, R. Arculus, and R. W. Kay, pp. 451–464, Elsevier, Amsterdam.

Holbrook, W. S., et al. (2001), Mantle thermal structure and melting processes during continental breakup in the North Atlantic, *Earth Planet. Sci. Lett.*, *190*, 251–266.

Hooft, E. E. E., B. Brandsdóttir, R. Mjelde, H. Shimamura, and Y. Murai (2006), Asymmetric plume-ridge interaction around Iceland: The Kolbeinsey Ridge Iceland seismic experiment, *Geochem. Geophys. Geosyst.*, *7*, Q05015, doi:10.1029/2005GC001123.

Hopper, J. R., T. Dahl-Jensen, W. S. Holbrook, H. C. Larsen, D. Lizarralde, J. Korenaga, G. M. Kent, and P. B. Kelemen (2003), Structure of the SE Greenland margin from seismic reflection and refraction data: Implications for nascent spreading center subsidence and asymmetric crustal accretion during North Atlantic opening, *J. Geophys. Res.*, *108*(B5), 2269, doi:10.1029/2002JB001996.

Ito, G., J. Lin, and D. Graham (2003), Observational and theoretical studies of the dynamics of mantle plume-mid-ocean ridge interaction, *Rev. Geophys.*, *41*(4), 1017, doi:10.1029/2002RG000117.

Jansen, E., et al. (1996), 8. Site 985, *Proc. Ocean Drill. Program Initial Rep.*, *162*, 253–283, doi:10.2973/odp.proc.ir.162.108.1996.

Johnson, G. L., and B. C. Heezen (1967), The morphology and evolution of the Norwegian-Greenland Sea, *Deep Sea Res. Oceanogr. Abstr.*, *14*, 755–771.

Johnson, G. L., and B. Tanner (1972), Geophysical observations on the Iceland-Faeroe Ridge, *Jökull*, *21*, 45–52.

Jones, S., N. White, and J. Maclennan (2002), V-shaped ridges around Iceland: Implications for spatial and temporal patterns of mantle convection, *Geochem. Geophys. Geosyst.*, *3*(10), 1059, doi:10.1029/2002GC000361.

Jung W., and P.R. Vogt (1997), A gravity and magnetic anomaly study of the extinct Aegir Ridge, Norwegian Sea, *J. Geophys. Res.*, *102*, 5065–5089.

Kanazawa T. and H. Shiobara (1994), Newly developed ocean bottom seismometer [in Japanese], *Program Abstr. Jpn. Earth Planet. Sci., Joint Meet.*, p. 341.
Keleman, P. B., and W. S. Holbrook (1995), Origin of thick, high-velocity igneous crust along the U.S. East Coast Margin, *J. Geophys. Res.*, *100*, 10,077–10,094.
Kharin, G. N. (1976), The petrology of magmatic rocks, DSDP leg 38, in *Initial reports Deep Sea Drilling Project*, vol. 38, pp. 685–715, U.S. Gov. Print. Off., Washington, D. C., doi:10.2973/dsdp.proc.38.110.1976.
Kharin, G. N., G. B. Udintsev, O. A. Bogatikov, J. I. Dmitriev, H. Raschka, H. Kreuzer, M. Mohr, W. Harre, and F. J. Eckhardt (1976), K/Ar ages of the basalts of the Norwegian-Greenland Sea DSDP leg 38, in *Initial reports Deep Sea Drilling Project*, vol. 38, pp. 755–759, U.S. Gov. Print. Off., Washington, D. C., doi:10.2973/dsdp.proc.38.116.1976.
Kodaira, S., R. Mjelde, K. Gunnarsson, H. Shiobara, and H. Shimamura (1998b), Evolution of oceanic crust on the Kolbeinsey Ridge, north of Iceland, over the past 22 Myr, *Terra Nova*, *10*, 27–31, doi:10.1046/j.1365-3121.1998.00166.x.
Kodaira, S., R. Mjelde, K. Gunnarsson, H. Shiobara, and H. Shimamura (1998a), Structure of the Jan Mayen micro-continent and implications for its evolution, *Geophys. J. Int.*, *132*, 383–400, doi:10.1046/j.1365-246x.1998.00444.x.
Korenaga, J. (2004), Mantle mixing and continental breakup magmatism, *Earth Planet. Sci. Lett.*, *218*, 463–473.
Korenaga, J., and W. W. Sager (2012), Seismic tomography of Shatsky Rise by adaptive importance sampling, *J. Geophys. Res.*, *117*, B08102, doi:10.1029/2012JB009248.
Korenaga, J., W. S. Holbrook, G. M. Kent, P. B. Kelemen, R. S. Detrick, H. C. Larsen, J. R. Hopper, and T. Dahl-Jensen (2000), Crustal structure of the southeast Greenland margin from joint refraction and reflection seismic tomography, *J. Geophys. Res.*, *105*, 21,591–21,614.
Korenaga, J., W. S. Holbrook, R. S. Detrick, and P. B. Kelemen (2001), Gravity anomalies and crustal structure at the southeast Greenland margin, *J. Geophys. Res.*, *106*, 8853–8876.
Korenaga, J., P. B. Kelemen, and W. S. Holbrook (2002), Methods for resolving the origin of large igneous provinces from crustal seismology, *J. Geophys. Res.*, *107*(B9), 2178, doi:10.1029/2001JB001030.
Kristjansson, L., K. Thors, and H. R. Karlsson (1977), Confirmation of central volcanoes off the Icelandic coast, *Nature*, *268*, 325–326.
Kuvaas B. and S. Kodaira (1997), The formation of the Jan Mayen microcontinent: The missing piece in the continental puzzle between the Møre-Vøring Basins and East Greenland, *First Break*, *15*(7), 239–247.
Larsen, H. C., and S. S. Jakobsdóttir (1988), Distribution, crustal properties and significance of seawards-dipping sub-basement reflectors off E Greenland, in *Early Tertiary Volcanism and the Opening of the NE Atlantic*, vol. 39, edited by A. C. Morton and L. M. Parson, pp. 95–114, Geol. Soc. Spec. Publ., London, U. K.
Larsen, H. C., and A. D. Saunders (1998), Tectonism and volcanism at the southeast Greenland rifted margin: A record of plume impact and later continental rifting, *Proc. Ocean Drill. Program Sci. Results*, *152*, 503–533.
Leftwich T. E., R. R. B. von Frese, L. V. Potts, H. Rae Kim, D. R. Romand, P. T. Taylor, and M. Barton (2005), Crustal modelling of the North Atlantic from spectrally correlated free-air and terrain gravity, *J. Geodyn.*, *40*, 23–50.
Lowrie, W. (1979), Geomagnetic reversals and ocean crust magnetization, in, *Deep Drilling Results in the Atlantic Ocean: Ocean Crust, Maurice Ewing Ser.*, edited by M. Talwani, C. G. Harrison and S. E. Hayes, vol. 2, pp. 135–150, AGU, Washington, D. C.
Menke, W., B. Brandsdóttir, P. Einarsson, and I. Bjarnason (1996), Reinterpretation of the RRISP-77 Iceland shear wave profiles, *Geophys. J. Int.*, *126*, 166–172.
Mertz, D. F., C. W. Devey, W. Todt, P. Stoffers, and A. W. Hoffman (1991), Sr-Nd-Pb isotope evidence against plume-asthenosphere mixing north of Iceland, *Earth Planet. Sci. Lett.*, *25*, 411–414.
Meyer, O., D. Voppel, U. Fleischer, H. Gloss, and K. Gerke (1972), Results of bathymetric, magnetic and gravimetric measurements between Iceland and 70°N, *Dtsch. Hydrogr. Z.*, *25*, 193–201.
Mjelde, R., R. Aurvåg, S. Kodaira, H. Shimamura, K. Gunnarsson, A. Nakanishi, and H. Shiobara (2002), V_P/V_S-ratios from the central Kolbeinsey Ridge to the Jan Mayen Basin, North Atlantic; implications for lithology, porosity and present-day stress field, *Mar. Geophys. Res.*, *23*, 125–145.
Mjelde, R., T. Raum, B. Myhren, H. Shimamura, Y. Murai, T. Takanami, R. Karpuz, and U. Nss (2005), Continent-ocean transition on the Vøring Plateau, NE Atlantic, derived from densely sampled ocean bottom seismometer data, *J. Geophys. Res.*, *110*, B05101, doi:10.1029/2004JB003026.
Mjelde, R., I. Eckhoff, S. Solbakken, S. Kodaira, H. Shimamura, K. Gunnarsson, A. Nakanishi, and H. Shiobara (2007), Gravity and S-wave modelling across the Jan Mayen Ridge, North Atlantic; implications for crustal lithology, *Mar. Geophys. Res.*, *28*, 27–41.
Mjelde, R., A.J. Breivik, T. Raum, E. Mittelstaedt, G. Ito, and J. I. Faleide (2008), Magmatic and tectonic evolution of the North Atlantic, *J. Geol. Soc. London*, *165*, 31–42.
Moser, T. J. (1991), Shortest path calculation of seismic rays, *Geophysics*, *56*, 59–67.
Moser, T. J., G. Nolet, and R. Snieder (1992), Ray bending revisited, *Bull. Seismol. Soc. Am.*, *82*, 259–288.
Müller, R. D., G. Gaina, W. R. Roest, and D. L. Hansen (2001), A recipe for microcontinent formation, *Geology*, *29*, 203–206.
Mutter, J. C., and C. M. Zehnder (1988), Deep crustal structure and magmatic processes: The inception of seafloor spreading in the Norwegian-Greenland Sea, in *Early Tertiary Volcanism and the Opening of the North Atlantic*, vol. 39, edited by A. C. Morton and L. M. Parson, pp. 35–4, Geol. Soc. Spec. Publ., London, U. K.
Mutter, J. C., W. R. Buck, and C. M. Zehnder (1988), Convective partial melting: 1. A model for the formation of thick basaltic sequences during the initiation of spreading, *J. Geophys. Res.*, *93*, 1031–1048.
Nielsen, T. K. and J. R. Hopper (2004), From rift to drift: Mantle melting during continental breakup, *Geochem. Geophys. Geosyst.*, *5*, Q07003, doi:10.1029/2003GC000662.
Norddahl, H., Inglfsson, H. G. Ptursson, and M. Hallsdttir (2008), Late Weichselian and Holocene environmental history of Iceland, *Jökull*, *58*, 343–364.
Nunns, A. (1982), The structure and evolution of the Jan Mayen Ridge and surrounding regions, in *Studies in Continental Margin Geology*, vol. 34, edited by J. S. Watkins and C. L. Drake, pp. 193–208, AAPG Mem., Tulsa, Oklahoma, USA.
Ogg, J. G. (2012), Geomagnetic Polarity Time Scale. *The Geologic Time Scale 2012*, vol. 2, pp. 85–113, Elsevier, Oxford, U. K.
Osler, J. C., and K. E. Louden (1995), Extinct spreading center in the Labrador Sea: Crustal structure from a two-dimensional seismic refraction velocity model. *J. Geophys. Res.*, *100*, 2261–2278.
Paige, C. C., and M. A. Saunders (1982), LSQR: An algorithm for sparse linear equations and least squares, *ACM Trans. Math. Software*, *8*, 43–71.
Pálmason, G. (1971), *Crustal Structure of Iceland From Explosion Seismology*, 187 pp., Soc. Sci. Island, Reykjavík, Iceland.
Parker, R. L., and S. P. Huestis (1974), The inversion of magnetic anomalies in the presence of topography, *J. Geophys. Res.*, *79*, 1587–1594.
Peron-Pinvidic, G., L. Gernigon, C. Gaina, and P. Ball (2012), Insights from the Jan Mayen system in the Norwegian-Greenland Sea: I. Mapping of a microcontinent, *Geophys. J. Int.*, *191*, 385–412, doi:10.1111/j.1365-246X.2012.05639.x.
Pitman, W. C. I., and M. Talwani (1972), Sea-floor spreading in the North Atlantic, *Geol. Soc. Am. Bull.*, *83*, 619–646.

Sæmundsson, K. (1986), Subaerial volcanism in the western North Atlantic, in *The Geology of North America, vol. M., The Western North Atlantic Region*, edited by P. R. Vogt and B. E. Tucholke, pp. 69–86, Geol. Soc. Am., Boulder, Colo.
Sandwell, D. T., and W. H. F. Smith, (1997), Marine gravity anomaly from Geosat and ERS1 satellite altimetry, *J. Geophys. Res.*, *102*, 10,039–10,054.
Schilling, J.-G. (1976), Rare-earth, Sc, Cr, Fe, Co, and Na abundances in DSDP leg 38 basement basalts: Some additional evidence on the evolution of the Thulean volcanic province, in *Initial Reports of the Deep Sea Drilling Project*, vol. 38, edited by T. M. and G. B. Udintsev, pp. 741–750, U.S. Gov. Print. Off., Washington, D. C., doi:10.2973/dsdp.proc.38.114.1976.
Shorttle, O., J. Maclennan, and S. Lambart (2014), Quantifying lithological variability in the mantle, *Earth Planet. Sci. Lett.*, *395*, 24–40. doi: 10.1016/j.epsl.2014.03.040.
Slater, L., D. McKenzie, K. Grönvold, and N. Shimizu (2001), Melt generation and movement beneath Theistareykir, NE Iceland, *J. Petrol.*, *42*, 321–354.
Sleep, N. H. (2007), Edge-modulated stagnant-lid convection and volcanic passive margins, *Geochem. Geophys. Geosyst.*, *8*, Q12004, doi: 10.1029/2007GC001672.
Smallwood, J. R., R. K. Staples, K. R. Richardson, R. S. White, and the FIRE Working Group (1999), Crust generated above the Iceland mantle plume: From continental rift to oceanic spreading center, *J. Geophys. Res.*, *104*, 22,885–22,902.
Srivastava, S. P., and C. R. Tapscott (1986), Plate kinematics of the North Atlantic, in *The Geology of North America, Vol. M, The Western North Atlantic Region*, pp. 379–404, Geol. Soc. of Am., Boulder, Colo.
Staples, R., R. S. White, B. Brandsdottir, W. Menke, P. Maguire, and J. McBride (1997), Färoe-Iceland Ridge Experiment 1. Crustal structure of northeastern Iceland, *J. Geophys. Res.*, *102*, 7849–7866.
Talwani, M., and O. Eldholm (1977), Evolution of the Norwegian-Greenland sea, *Geol. Soc. Am. Bull.*, *88*, 969–999.
Talwani, M., and G. B. Udintsev (1976), Tectonic synthesis, in *Initial Reports of the Deep Sea Drilling Project*, vol. 38, edited by M. Talwani and G. B. Udintsev, pp. 1213–1242, U.S. Gov. Print. Off., Washington, D. C., doi:10.2973/dsdp.proc.38.134.1976.
Toomey, D. R., G. M. Purdy, S. C. Solomon, and W. S. D. Wilcock (1990), The three-dimensional seismic velocity structure of the East Pacific Rise near latitude 9°30′N, *Nature*, *347*, 639–645.
Vogt, P. R., and O. E. Avery (1974), Detailed magnetic surveys in the Northeast Atlantic and Labrador Sea, *J. Geophys. Res.*, *79*, 363–389.
Vogt, P. R., N. A. Ostenso, and G. L. Johnson (1970), Magnetic and bathymetric data bearing on seafloor spreading north of Iceland, *J. Geophys. Res.*, *75*, 903–920.
Vogt, P. R., G. L. Johnson, and L. Kristjansson (1980), Morphology and magnetic anomalies north of Iceland, *J. Geophys. Res.*, *47*, 67–80.
Wallrabe-Adams, H. J., and R. Werner (1999), 16. Data report: Chemical composition of middle Miocene-lower Pliocene ash from sites 982 and 985, *Proc. ODP Sci. Res*, *162*, 217–230, doi:10.2973/odp.proc.sr.162.021.1999.
Weigel, W. E., et al., (1995), Investigations of the East Greenland continental margin between 70° and 72° N by deep seismic sounding and gravity studies, *Mar. Geophys. Res.*, *17*, 167–199.
Weir, N., R. S. White, B. Brandsdóttir, P. Einarsson, H. Shimamura, and H. Shiobara (2001), Crustal structure of the northern Reykjanes Ridge and Reykjanes Peninsula, south-west Iceland, *J. Geophys. Res.*, *106*, 6347–6368.
Wessel, P., and W. H. F. Smith (1991), Free software helps map and display data, *Eos Trans. AGU*, *72*(441), 445–446.
White, R. S. (1992), Crustal structure and magmatism of North Atlantic continental margins, *J. Geol. Soc.*, *149*, 841–854.
White, R. S., and L. K. Smith (2009), Crustal structure of the Hatton and the conjugate east Greenland rifted volcanic continental margins, NE Atlantic, *J. Geophys. Res.*, *114*, B02305, doi:10.1029/2008JB005856.
White, R. S., L. K. Smith, A. W. Roberts, P. A. F. Christie, N. J. Kusznir, and the rest of the iSIMM Team (2008), Lower crustal intrusion on the North-Atlantic continental margin, *Nature*, *452*, 460–464, doi:10.1038/nature06687.